

Scale-invariant Gaussian derivative residual networks

Andrzej Perzanowski and Tony Lindeberg

Abstract Generalisation across image scales remains a fundamental challenge for deep networks, which often fail to handle images at scales not seen during training (the out-of-distribution problem). In this paper, we present provably scale-invariant Gaussian derivative residual networks (GaussDerResNets), constructed out of scale-covariant Gaussian derivative residual blocks coupled in cascade, aimed at addressing this problem.

By adding residual skip connections to the previous notion of Gaussian derivative layers, deeper networks with substantially increased accuracy can be constructed, while preserving very good scale generalisation properties at the higher level of accuracy. Explicit proofs are provided regarding the underlying scale-covariant and scale-invariant properties in arbitrary dimensions. We also conceptually relate the functionality of the Gaussian derivative residual blocks to semi-discretisations of the velocity-adapted affine diffusion equation.

To analyse the ability of GaussDerResNets to generalise to new scales, we apply them on the new rescaled version of the STL-10 dataset, where training is done at a single fixed scale and evaluation is performed on multiple copies of the test set, each rescaled to a single distinct spatial scale, with scale factors extending over a range of 4. We also conduct similar systematic experiments on the rescaled versions of Fashion-MNIST and CIFAR-10 datasets introduced in our previous work.

The support from the Swedish Research Council (contract 2022-02969) is gratefully acknowledged.

Andrzej Perzanowski (corresponding author)
amper@kth.se

Tony Lindeberg
tony@kth.se

Computational Brain Science Lab, Department of Computational Science and Technology, KTH Royal Institute of Technology, SE-100 44 Stockholm, Sweden.

Experimentally, we demonstrate that the GaussDerResNets have strong scale generalisation and scale selection properties, while also achieving good test accuracy, on all the three rescaled datasets. In our ablation studies, we investigate different architectural variants of GaussDerResNets, demonstrating that basing the architecture on depthwise-separable convolutions allows for decreasing both the number of parameters and the amount of computations, with reasonably maintained accuracy and scale generalisation. We also find that including a zero-order Gaussian term in the layer definition can sometimes be beneficial, as demonstrated for our spatial-max-pooling-based networks trained on the rescaled STL-10 dataset.

In these ways, we demonstrate how deep networks can in a theoretically well-founded way handle variations in scale in the testing data that are not spanned by the training data.

Keywords Scale covariance · Scale invariance · Scale generalisation · Scale selection · Gaussian derivative · Scale space · Residual networks · Deep learning

1 Introduction

To effectively process real-world images acquired under general viewing conditions, deep networks in computer vision must be capable of handling scaling transformations over the spatial domain, since the size of an object in the image domain may differ, both because the different physical dimensions of the 3-D objects in the world and variations in the distance to the camera.

A theoretically well-founded way of incorporating priors about spatial scaling transformations into convolutional neural networks (CNNs) is by requiring the networks to be *scale covariant*, also referred to as scale equivariant, see Worrall and Welling (2019), Bekkers

(2020), Sosnovik et al. (2020, 2021), Zhu et al. (2022), Jansson and Lindeberg (2022), Lindeberg (2022), Zhan et al. (2022), Wimmer et al. (2023) and Perzanowski and Lindeberg (2025c) for introductory overviews.

Such scale covariance extends the built-in inductive bias of regular CNNs regarding translational covariance, which enforces the application of the same filter at the every spatial location in an image, to also comprise structurally similar processing operations at different scales, by expanding the sizes of the receptive fields in the networks over substantial scaling variations. This guarantees that a spatially shifted input produces a correspondingly shifted activation map in each layer, as well as that a spatially rescaled image pattern invokes a similar response in a transformed scale layer in the network.

A particular desirable property of a scale-covariant network is the ability to perform *scale generalisation*, to perform testing at scales that are not spanned by the training data. A regular, not scale-covariant, network will, in general, perform very poorly if exposed to such scale generalisation tasks. A theoretical explanation for this is that regular deep networks without complementary priors merely perform interpolation between the training data, with very poor abilities to perform extrapolation (Domingos 2020, Courtois et al. 2023).

To some extent, one could conceive the ability to process image data at different scales to be improved by performing data augmentation (Zhong et al. 2025), by substantially increasing the amount of training data with artificially rescaled images. It is, however, not clear how effective such an approach would be, when applied to testing data over wide scale ranges. For evaluating the scale-covariant properties of a deep network architecture, it is therefore essential to explore its scale generalisation abilities, when applied to testing data at scales that are not spanned by the training data.

Additionally, from the viewpoint of a vision system that learns to recognise objects from visual data, one may question whether it should be necessary to see a new object from all the distances from which it is later going to be recognised. Instead, the philosophy that we follow here is that it should be sufficient to see a new object from a single distance, by providing priors about scaling transformations to the deep network architecture, that enable generalisation to new scales that are not spanned by the training data.

In previous work, we have developed a particular architecture for scale-covariant deep networks with the layers defined from linear combinations of Gaussian derivative operators over multiple scales (Lindeberg 2022, Perzanowski and Lindeberg 2025c). This approach extends ideas from classical scale-space theory, where Gaussian

smoothing and Gaussian derivatives at multiple scales have been axiomatically shown to constitute a canonical class of filters for processing image data (Iijima 1962, Koenderink 1984, Koenderink and van Doorn 1992, Lindeberg 1993; 2011, Weickert et al. 1999). This approach is also closely related to other work on using Gaussian derivative operators as the computational primitives in deep networks, see Jacobsen et al. (2016), Pintea et al. (2021), Penaud-Polge et al. (2022), Gavilima-Pilataxi and Ibarra-Fiallo (2023) and Basting et al. (2024).

Concerning the more general use of Gaussian derivative operators as computational primitives in deep networks, it is also notable that by applying a greedy clustering technique to the receptive fields learned from depthwise-separable deep networks, Babaiee *et al.* (2024b, 2024a, 2025), have extracted a set of “8 master key filters” from the ConvNeXt V2 Tiny model developed by Woo *et al.* (2023) and Liu *et al.* (2022), and which have been shown to be well modelled in terms of discrete scale-space filters, see Lindeberg et al. (2025).

By the provable scale-covariant and scale-invariant properties of the Gaussian derivative networks (GaussDerNets) in Lindeberg (2022) and Perzanowski and Lindeberg (2025c), these networks were demonstrated to have very good scale generalisation properties, with structurally very close similarities to classical methods for automatic scale selection (Lindeberg 1998a; 1998b; 2013c; 2015; 2021b, Bretzner and Lindeberg 1998, Lowe 2004, Bay et al. 2008).

The subject of this article is to extend this class of deep networks to incorporate residual skip connections (He et al. 2016), which will make it possible to construct deeper GaussDerNets, without encountering training problems due to vanishing gradients when increasing the number of layers. Experimentally, we will demonstrate that this approach leads to a significant increase in the accuracy of the resulting Gaussian derivative residual ResNets (GaussDerResNets), to a level more comparable to modern ResNets. We will also demonstrate that the presented approach can be combined with the notion of depthwise-separable networks (Chollet 2017, Howard *et al.* 2017) to formulate depthwise-separable Gaussian derivative residual networks (DS-GaussDerResNets), that substantially reduce the amount of computations, by decoupling the convolution operations across the layers in the networks from the spatial convolutions.

Specifically, we will show that this extension from GaussDerNets to GaussDerResNets, as well as further to DSGaussDerResNets architectures, can be performed with maintained and even improved scale covariance, scale invariance and scale generalisation properties, for

our resulting discrete implementations of the continuously formulated network architecture.

1.1 Contributions and novelty

To summarise, the main contributions of this paper comprise:

- Extension of the regular GaussDerNet architecture to GaussDerResNets.
- A general proof in arbitrary dimensions that the resulting GaussDerResNet architecture is scale covariant for arbitrary orders of spatial differentiation.
- Qualitative relationships between the proposed Gaussian derivative residual blocks and semi-discretisations of the velocity-adapted affine diffusion equation.
- Experimental evaluation of single-scale GaussDerResNets on the regular STL-10 dataset.
- Experimental evaluation of the scale generalisation properties of multi-scale GaussDerResNets, when applied to the previously existing Rescaled Fashion-MNIST dataset and the Rescaled CIFAR-10 dataset.
- Experimental evaluation of the scale generalisation properties of the GaussDerResNets when applied to new Rescaled STL-10 dataset proposed here.
- Ablation studies regarding:
 - the extension of GaussDerResNets to depthwise-separable GaussDerResNets, to reduce both the number of parameters and the amount of computations in the network with reasonably maintained accuracy and scale generalisation properties,
 - including a zero-order term in the Gaussian derivative residual layers in the higher layers of the GaussDerResNets, which will be demonstrated to improve the performance on the rescaled STL-10 dataset,
 - effects of pre-training with a single-scale-channel network to improve the efficiency and convergence of the training process, while significantly improving the scale generalisation at finer scales,
 - showing that weight transfer to a network with a denser scale-channel count can provide minor improvements to scale generalisation, without any additional training cost, and
 - using label smoothing to improve the convergence properties of the training process.

In these ways, we substantially extend the framework for GaussDerNets in Lindeberg (2022) as well as the extended GaussDerNets in Perzanowski and Lindeberg (2025c) to wider applicability in deeper GaussDerResNets, which have significantly better performance in

terms of accuracy and scale generalisation, when applied to datasets with more complex image structures.

Finally, we inspect the activation maps and the learned filters of the network, to better understand how the GaussDerResNets operate, as the architecture makes these visualisations very interpretable.

2 Related work

Initial efforts to develop scale-invariant deep networks for vision were undertaken by Xu et al. (2014), Kanazawa et al. (2014), Marcos et al. (2018) and Ghosh and Gupta (2019). Hierarchical networks that handle spatial scaling variations have also been developed by Bruna and Mallat (2013) and Mallat (2016) based on wavelet operations in terms of scattering transforms, and by Lindeberg (2020) based on structurally related idealised models of complex cells, in terms of quasi quadrature combinations of first- and second-order Gaussian derivatives.

Other approaches to involving multiple spatial scales in deep networks have been developed by Chen et al. (2019) in terms of octave convolution, by Xu et al. (2020) in terms of blur integrated gradients, by Wang et al. (2020) in terms of scale-equalising pyramid convolution, by Singh et al. (2022) regarding scale-normalised image pyramids, by Fu et al. (2022) to reduce scale differences for large scale image matching, by Wolski et al. (2024) using learning across scales with adversarial training, and by Zhang et al. (2025) using a scale- and rotation-handling retina-like image transformation. Rahman et al. (2025) proposed to include canonicalisers, to make pretrained networks scale equivariant. Xu et al. (2025) proposed a method for object counting to handle size variations in the image data. Cho et al. (2025) proposed a scale-equivariant network for object perception in autonomous driving.

Beyond the scale-covariant deep network architectures by Worrall and Welling (2019), Bekkers (2020), Sosnovik et al. (2020, 2021), Zhu et al. (2022), Jansson and Lindeberg (2022), Lindeberg (2022), Zhan et al. (2022), Wimmer et al. (2023) and Perzanowski and Lindeberg (2025c) mentioned in the introduction, scale-covariant U-Nets have been developed by Sangalli et al. (2022b) and Yang et al. (2022), scale-invariant Riesz networks by Barisin et al. (2024a; 2024b), and more recently scale-invariant HMAX networks based on trainable filters by Pant et al. (2024).

There have also been approaches for equivariant or invariant learning developed by Bruintjes et al. (2023), Mondal et al. (2023), van der Ouderaa et al. (2023), Moskalev et al. (2023), Shewmake et al. (2023), Pertigkiozoglou et al. (2024), Nordenfors and Flinth (2024),

Perin and Deny (2025) and Manolache et al. (2025). It is, however, not clear to what extent such learning-based approaches to covariance or invariance properties would allow for scale generalisation to scale levels that are not spanned in the training stage of the network.

The Gaussian smoothing and Gaussian derivative filters in the deep networks developed by Jacobsen et al. (2016), Pintea et al. (2021), Lindeberg (2022), Sangalli et al. (2022b, 2022a), Penaud-Polge et al. (2022), Gavilima-Pilataxi and Ibarra-Fiallo (2023), Basting et al. (2024) and Perzanowski and Lindeberg (2025c) satisfy the diffusion equation. In this respect, these methods have close structural similarities to other deep networks modelled by partial differential equations.

Indeed, deep learning has seen a shift in perspective, with architectures, such as ResNets (He et al. 2016), having an alternative interpretation of being numerical discretisations of partial differential equations, see Ruthotto and Haber (2020) and Lu et al. (2018). This connection has been further explored by Alt et al. (2023), who show that there are close structural parallels between numerical algorithms for partial differential equations (PDEs) and certain neural network architectures, such as ResNets. Furthermore, PDE-based networks that generate scale spaces have been proposed by Smets et al. (2023) and Bellaard et al. (2025).

Recently, ResNets have been developed to mimic the properties of visual transformers, see Dai et al. (2021), Liu et al. (2022) and Rao et al. (2021).

More generally, the development of scale-covariant architectures for deep learning is part of wider effort of geometric deep learning (Bronstein et al. 2021, Gerken et al. 2023), by incorporating explicit modelling of the influence of geometric image transformations on the receptive field responses (Lindeberg 2021a, 2023, 2025b).

3 Gaussian derivative residual networks

In this section, we will first define the computational primitives in scale-covariant and scale-invariant GaussDerResNets, as combinations of notions in scale-covariant and scale-invariant GaussDerNets (Lindeberg 2022, Perzanowski and Lindeberg 2025c) and ResNets (He et al. 2016). Then, we will show that the resulting networks, obtained by coupling these computational primitives in cascade, will be provably scale covariant. Finally, we will combine these network primitives with joint selection mechanisms over space and scale, to express scale-invariant deep network architecture for image classification tasks similar to object recognition.

3.1 Scale covariance property for Gaussian derivative layers with residual skip connections

In Lindeberg (2022), it was shown that regular GaussDerNets, obtained by coupling layers based on linear combinations of Gaussian derivative operators in cascade, are provably scale covariant. In this section, we will show that Gaussian derivative layers complemented by residual skip connections are also provably scale covariant. In relation to the previous proof in Lindeberg (2022), which was performed for GaussDerNets of order 2 for 2-D image data, we will here provide a more general proof, which applies to GaussDerResNets of any order N and for any dimensionality D of the input data.

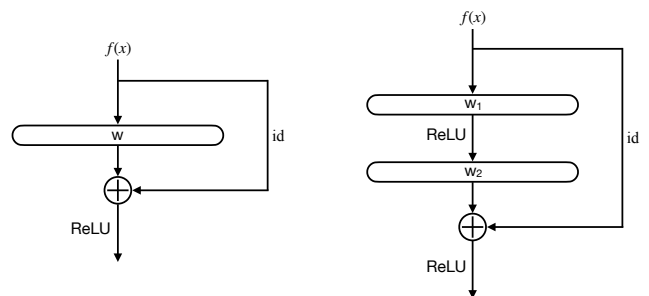


Fig. 1: Schematic illustrations of simplified residual blocks: **(left)** the simplest possible residual block of the form (1), based on a single convolution kernel w , **(right)** the basic residual block of the form (2), based on two convolution kernels w_1 and w_2 . In both the diagrams, the skip connections perform identity mappings on the input $f(x)$, denoted as id .

3.1.1 Prerequisites

The fundamental building block in a GaussDerResNet is the combination of an input function $f: \mathbb{R}^D \rightarrow \mathbb{R}$ denoted $f(x)$ for $x = (x_1, x_2, \dots, x_D)^T \in \mathbb{R}^D$ with a convolution kernel $w: \mathbb{R}^D \rightarrow \mathbb{R}$, a pointwise ReLU function $\text{ReLU}: \mathbb{R} \rightarrow \mathbb{R}$ and a skip connection of the form illustrated in Figure 1 (left)

$$M(x) = \text{ReLU}(f(x) + (w * f)(x)). \quad (1)$$

More generally, one could also combine several convolution kernels, say $w_1(x)$ and $w_2(x)$, of the form illustrated in Figure 1 (right)

$$M(x) = \text{ReLU}(f(x) + w_2 * \text{ReLU}((w_1 * f))(x)). \quad (2)$$

Since the logical structure is essentially the same, we will in the logical steps of the proof consider residual skip connections of the form (1).

Let us next, inspired by the structure of regular GaussDerNets, assume that the convolution kernel $w(x)$

in (1) is a linear combination of Gaussian derivative operators of the form

$$w(x; \sigma) = \sum_{\alpha: |\alpha| \leq N} m(\alpha) C_\alpha \sigma^{|\alpha|} g_{x^\alpha}(x; \sigma), \quad (3)$$

where

- $\alpha = (\alpha_1, \alpha_2, \dots, \alpha_D) \in \mathbb{Z}^D$ is a multi-index in D dimensions,
- $|\alpha| = \alpha_1 + \alpha_2 + \dots + \alpha_D \in \mathbb{Z}$ represents the total order of differentiation as the sum of the indices,
- $m(\alpha) = \binom{|\alpha|}{\alpha_1 \alpha_2 \dots \alpha_D} \in \mathbb{R}$ is a multinomial normalisation factor between different orders α of spatial differentiation, similar to the coefficients in a Taylor expansion of the same order $|\alpha|$,
- $g_{x^\alpha}(x; \sigma)$ is a D -dimensional Gaussian derivative kernel of order α at the scale $\sigma \in \mathbb{R}_+$ according to

$$g_{x^\alpha}(x; \sigma) = \partial_{x^\alpha} g(x; \sigma) \quad (4)$$

for

$$g(x; \sigma) = \frac{1}{\sqrt{2\pi}^D} e^{-x^T x / 2\sigma^2} \quad (5)$$

and $\partial_{x^\alpha} = \partial_{x_1^{\alpha_1} x_2^{\alpha_2} \dots x_D^{\alpha_D}}$,

- $N \in \mathbb{Z}_+$ denotes the maximum order of spatial differentiation for the Gaussian derivative kernels, and
- the coefficients $C_\alpha \in \mathbb{R}$ denote the filter weights¹ to be learned. In general, these weights will be different for different layers in the network. The weights will, however, be shared between different scale channels, corresponding to using different values of the initial scale level $\sigma_0 \in \mathbb{R}_+$ in the first layer of the network.

For example, for a Gaussian derivative layer of the form (3) of order 2, we should for 2-D input data let the multi-index α loop over the set

$$\alpha \in \{(1, 0), (0, 1), (2, 0), (1, 1), (0, 2)\}. \quad (6)$$

Similarly, for a Gaussian derivative layer of order 3, we should for 2-D input data let the multi-index α loop

over the set

$$\alpha \in \{(1, 0), (0, 1), (2, 0), (1, 1), (0, 2), \dots, (3, 0), (2, 1), (1, 2), (0, 3)\}. \quad (7)$$

Figure 2 shows examples of such primitive Gaussian derivative kernels up to order 3 in the 2-D case.

The functionality of the scale normalisation factor $\sigma^{|\alpha|}$ in (3) is to ensure that the Gaussian derivative operators are properly normalised over scale according to Lindeberg (1998b) for the most scale-invariant choice of the scale normalisation power $\gamma = 1$, as the scale parameter σ may be varied between different scale channels in the network for different values of σ .

3.1.2 Transformation property under spatial scaling transformations

Let us next consider the effect of scaling transformations applied to a minimal Gaussian derivative residual block of the form

$$M(x; \sigma) = (\mathcal{M}_\sigma f)(x; \sigma) = \text{ReLU}(f(x) + (w(\cdot; \sigma) * f(\cdot))(x)), \quad (8)$$

where

- $M(\cdot; \sigma)$ denotes the layer at scale σ ,
- \mathcal{M}_σ denotes the operator that computes the layer from the input f , and with
- the convolution kernel $w(x; \sigma)$ now of the form (3).

Thus, given rescaled input data $f'(x')$ defined according to

$$f'(x') = f(x) \quad \text{for} \quad x' = Sx, \quad (9)$$

where $S \in \mathbb{R}_+$ is a spatial scaling factor, we define the output from a corresponding transformed Gaussian derivative residual layer as

$$M'(x'; \sigma') = (\mathcal{M}_{\sigma'} f')(x'; \sigma') = \text{ReLU}(f'(x') + (w'(\cdot; \sigma') * f'(\cdot))(x')), \quad (10)$$

where the transformed convolution kernel is of the form

$$w'(x'; \sigma') = \sum_{\alpha: |\alpha| \leq N} m(\alpha) C_\alpha \sigma'^{|\alpha|} g_{x^\alpha}(x'; \sigma'), \quad (11)$$

specifically using the same filter weights C_α as in the definition of $w(x; \sigma)$ in (3), to enable spatial scale covariance.

Then, from a previously established property (Lindeberg 1998b), further detailed in Equation (15) below, that scale-normalised Gaussian derivative responses are equal at corresponding image points

¹ Note that, in order to simplify the notation, we here normalise the filter weights in a different way than in the original work on scale-covariant and scale-invariant Gaussian derivative networks (Lindeberg 2022). Since the filter weights are anyway to be learned, the choice of the normalisation method for the filter weights does, however, not affect the functional properties of the network. In the original definition of the Gaussian derivative networks for 2-D image data, the filter coefficients are instead normalised with C_α here replaced by $m(\alpha) C_\alpha$, with $m(\alpha) = \binom{|\alpha|}{\alpha_1 \alpha_2}$ denoting the binomial coefficient arising in a corresponding Taylor expansion of the same order. For higher-dimensional input functions, the normalisation factor $m(\alpha) = \binom{|\alpha|}{\alpha_1 \alpha_2 \dots \alpha_D}$ should instead correspond to a corresponding multinomial coefficient in D dimensions.

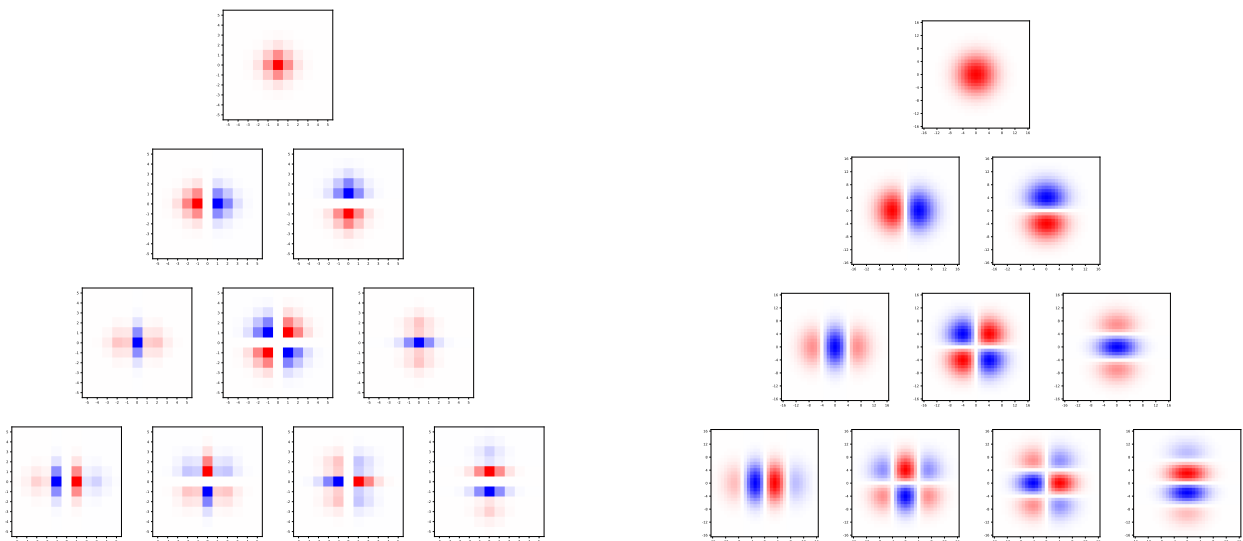
(a) Discrete Gaussian derivative kernels for $\sigma = 1$.(b) Discrete Gaussian derivative kernels for $\sigma = 4$.

Fig. 2: Discretised Gaussian derivative kernels up to order 3, for (left) the scale parameter $\sigma = 1$ and for (right) the scale parameter $\sigma = 4$. These receptive fields are obtained by applying central difference operators (corresponding to the given derivative order) to the discrete analogue of the Gaussian kernel, as defined in Equation (59). The ranges of both the axes of the filters are for (the left figure) in the interval $[-5, 5]$, and for (the right figure) in the interval $[-16, 16]$. **(Top row)** the zero-order Gaussian kernel $g(x_1, x_2; \sigma)$, **(second row)** first-order Gaussian derivatives $g_{x_1}(x_1, x_2; \sigma)$ and $g_{x_2}(x_1, x_2; \sigma)$, **(third row)** second-order Gaussian derivatives $g_{x_1x_1}(x_1, x_2; \sigma)$, $g_{x_1x_2}(x_1, x_2; \sigma)$, $g_{x_2x_2}(x_1, x_2; \sigma)$, **(bottom row)** third-order Gaussian derivatives $g_{x_1x_1x_1}(x_1, x_2; \sigma)$, $g_{x_1x_1x_2}(x_1, x_2; \sigma)$, $g_{x_1x_2x_2}(x_1, x_2; \sigma)$ and $g_{x_2x_2x_2}(x_1, x_2; \sigma)$.

$$\begin{aligned} \left(\left(\sigma^{|\alpha|} g_{x^\alpha}(\cdot; \sigma') \right) * f'(\cdot) \right) (x'; \sigma') &= \\ &= \left(\left(\sigma^{|\alpha|} g_{x^\alpha}(\cdot; \sigma) \right) * f(\cdot) \right) (x; \sigma), \end{aligned} \quad (12)$$

provided that the scale values σ and σ' are properly matched according to

$$\sigma' = S\sigma, \quad (13)$$

it follows that the output from the Gaussian derivative residual layers will be equal

$$M'(x'; \sigma') = M(x; \sigma), \quad (14)$$

provided that the scale parameters σ and σ' are properly matched according to (13).

The relationship (12) can also with more standard notation for Gaussian derivative responses be written as

$$L'_{\xi^\alpha}(x'; \sigma') = L_{\xi^\alpha}(x; \sigma) \quad (15)$$

with

$$L_{\xi^\alpha}(x; \sigma) = \left(\left(\sigma^{|\alpha|} g_{x^\alpha}(\cdot; \sigma) \right) * f(\cdot) \right) (x; \sigma), \quad (16)$$

$$L'_{\xi^\alpha}(x'; \sigma') = \left(\left(\sigma'^{|\alpha|} g_{x^\alpha}(\cdot; \sigma') \right) * f'(\cdot) \right) (x'; \sigma'), \quad (17)$$

where $L_{\xi^\alpha}(x; \sigma)$ and $L'_{\xi^\alpha}(x'; \sigma')$ denote the regular scale-normalised Gaussian derivative responses computed

for the functions $f(x)$ and $f'(x')$, respectively. With this notation, the equality in Equation (15) follows from Equation (25) in Lindeberg (1998b) for the choice of the scale normalisation power $\gamma = 1$.

3.1.3 Generalisation to more general forms of skip connections in composed Gaussian derivative residual networks

In this way, we have shown that a maximally simplified Gaussian derivative residual block of the form (8) is scale covariant. Since the pointwise ReLU function does not affect the scale covariance properties, and additionally all the primitive components in the residual block (8) are provably scale covariant, it follows that also a more composed residual block of the form illustrated in Figure 1 (right)

$$\begin{aligned} M(x; \sigma) &= (\mathcal{M}_\sigma f)(x; \sigma) = \\ &= \text{ReLU}(f(x) + (w_2(\cdot; \sigma) * \text{ReLU}(w_1(\cdot; \sigma) * f(\cdot))))(x) \end{aligned} \quad (18)$$

with the two convolution kernels $w_1(x; \sigma)$ and $w_2(x; \sigma)$ of the form (3) will be scale covariant. Thereby, we can freely make use of residual skip connections in the proposed class of GaussDerResNets, with maintained scale covariance properties.

Additionally, because of the scale covariance property of a single composed Gaussian derivative residual block, it holds that the scale covariance property also applies to the coupling of multiple Gaussian derivative residual blocks in cascade, provided that the values of the scale parameters are appropriately matched between the layers in the corresponding scale channels.

Finally, concerning the generality of this scale covariance property, it should be remarked that this result is not specific to pointwise transformations of the ReLU form, but applies to more general classes of pointwise transformations of the output from each convolution stage. Furthermore, since a batch normalisation stage does neither affect the scale covariance properties, the scale covariance property does also apply with batch normalisation stages between the layers.

3.2 Connections between Gaussian derivative residual blocks and semi-discretisations of the diffusion equation

Smoothing of any image f with the Gaussian kernel, as used for computing the Gaussian derivative responses in the Gaussian derivative layers and the Gaussian derivative residual layers, according to

$$L(\cdot; s) = g(\cdot; s) * f(\cdot), \quad (19)$$

for the scale parameter in units of the variance $s = \sigma^2$ of the Gaussian kernel, corresponds to a solution of the diffusion equation

$$\partial_s L = \frac{1}{2} \nabla^2 L = \frac{1}{2} (\partial_{x_1 x_1} + \partial_{x_2 x_2} + \dots + \partial_{x_D x_D}) \quad (20)$$

with initial condition $L(\cdot; 0) = f(\cdot)$.

If we discretise this diffusion equation along the scale direction s only, according to Euler's forward method

$$(\partial_s L)(\cdot; s) \approx \frac{L(\cdot; s + \Delta s) - L(\cdot; s)}{\Delta s}, \quad (21)$$

then this corresponds to a forward iteration of the form

$$L(\cdot; s + \Delta s) = \left(1 + \frac{\Delta s}{2} \nabla^2 \right) L(\cdot; s). \quad (22)$$

As earlier pointed out in more general terms by Alt et al. (2023), there is a close structural similarity between this form of computational operation and the skip connections in a ResNet.

In our case with Gaussian derivative residual layers, this computational operation is, however, different in the sense that the representations that we compute are, however, not mere Gaussian smoothing operations

or computations of the form “1 + a Laplacian increment”. Instead, we use linear combinations of Gaussian derivative responses of different orders, which then constitute a way of parametrising a set of degrees of freedom in a computational operation of the form “1 + correction”, with these degrees of freedom specifically corresponding to a Taylor expansion of the local image structure at a certain scale for a non-linear operation of the simplest possible form of a Gaussian derivative residual block according to

$$\begin{aligned} M(\cdot; \sigma) &= \\ &= \text{ReLU} \left(\left(1 + \sum_{\alpha: |\alpha| \leq N} m(\alpha) C_\alpha \sigma^{|\alpha|} \partial_{x^\alpha} g(\cdot; \sigma) \right) * M(\cdot; 0) \right). \end{aligned} \quad (23)$$

For the special case when the maximum differentiation order $N = 2$, and if we disregard the effect of the non-linear ReLU operation and the Gaussian smoothing operation $g(\cdot; \sigma)$, it holds that this evolution operation corresponds to the first step of evolution in a semi-discretisation in the scale direction of the D -dimensional velocity-adapted affine diffusion equation (Lindeberg 2011 Equation (27))

$$\partial_s L = \frac{1}{2} \nabla^T (\Sigma \nabla L) - v^T \nabla L \quad (24)$$

with the spatial covariance matrix Σ of size $D \times D$, the D -dimensional velocity vector v , and the step size Δs

$$L(\cdot; s + \Delta s) = \left(1 + \Delta s \left(\frac{1}{2} \nabla^T \Sigma \nabla - v^T \nabla \right) \right) L(\cdot; s) \quad (25)$$

for the specific choice of the elements of the spatial covariance matrix $\Sigma = \{\Sigma_{i,j}\}_{i=1..D, j=1..D}$ and the velocity vector $v = \{v_i\}_{i=1..D}$ obeying

$$\Delta s \Sigma_{i,j} = C_{i,j} \sigma^2, \quad (26)$$

$$\Delta s v_i = C_i \sigma. \quad (27)$$

Here, we have implicitly assumed natural rules for converting the multi-index notion for the first-order Taylor coefficients with multi-index notation C_α for $|\alpha| = 1$ to explicitly indexed values C_i and for converting the second-order Taylor coefficients with multi-index notation C_α for $|\alpha| = 2$ to explicitly indexed values $C_{i,j}$.

In this respect, there is a direct connection between the differential structure in the maximally simplified primitive Gaussian derivative residual block of the general form (8), specialised to the form (23), and generalised models of spatial receptive fields according to

the theory in Lindeberg (2011), which can be precisely shown to correspond to constitute solutions of generalised diffusion equations of the form (24).

Additionally, the representations in the implementation are further regularised by a complementary spatial discretisation, as well as complementary discrete spatial smoothing steps with isotropic discrete Gaussian kernels, when computing the spatial derivatives underlying the discrete iteration over Gaussian derivative residual layers. By the use of such significantly non-infinitesimal amounts of spatial smoothing in the computation of the spatial derivative responses, the influence of fine-scale and high-frequency image structures on the scale steps will be fundamentally different from the bounds on the scale step Δs obtained when not using such complementary spatial smoothing in the computation of spatial derivatives in more classical explicit forward schemes for the diffusion equation. Due to the use of isotropic Gaussian smoothing as the spatial smoothing operation in these iterations, the resulting GaussDerResNet architecture implied by the Gaussian derivative residual blocks of the form (23) will, however, not obey similar affine covariant properties as the velocity-adapted affine diffusion equation (24).

3.3 Resulting Gaussian derivative ResNet architecture

Based on the above theory, we propose to define GaussDerResNets by coupling sets of Gaussian derivative residual layers in cascade, with non-linearities in between. For this purpose, we consider two main types of architectures:

- a single-scale-channel network, also referred to as a scale channel, constructed from a given choice of the initial scale level σ_0 , illustrated in Figure 3, and
- a multi-scale-channel network, constructed from an expansion over multiple initial scale levels $\sigma_{n,0}$ for each scale channel indexed by $n \in \mathbb{Z}$, which we introduce in Section 3.6, and illustrate in Figure 5.

Notably, when constructing the GaussDerResNets, the first and the last layers are regular Gaussian derivative layers without skip connections, while all the intermediate layers are Gaussian derivative residual layers with skip connections, as also illustrated in Figure 3.

The reason, for using a regular Gaussian derivative layer, instead of a Gaussian derivative residual layer in the first layer, is that regular Gaussian derivative kernels have by axiomatic derivations been shown to constitute a canonical choice for defining the first layer of visual processing, based on general symmetry arguments by Iijima (1962), Koenderink (1984), Koenderink

and van Doorn (1992), Lindeberg (1993; 2011) and Weickert et al. (1999). By this choice, we also prevent the pure input image from being forwarded to the higher layers by skip connections. The reason, for using a regular Gaussian derivative layer instead of a Gaussian derivative residual layer in the last layer, is to provide maximum flexibility with respect to the construction of the output from each single scale channel. These choices are also consistent with how regular ResNets, not based on Gaussian derivatives, are constructed, by not using any skip connections in the first or the last layers.

In the following, we will use the index κ for indicating the number of each layer in the 18-layer GaussDerResNet that we will consider henceforth. Specifically, since for the Gaussian derivative residual layers, the two consecutive Gaussian derivative layers within each residual block have the same values of the scale parameters of their spatial weighting functions, we also define the effective layer number k as

$$k = \lfloor \frac{\kappa}{2} \rfloor + 1 = \frac{\kappa - (\kappa \bmod 2)}{2} + 1 \quad (28)$$

where $\lfloor \cdot \rfloor$ denotes the floor rounding function. This means that the individual Gaussian derivative layers are indexed by κ , while the residual blocks use the index k .

For practical purposes, we typically choose the successively higher scale levels $\sigma_k \in \mathbb{R}_+$ in the cascade of Gaussian derivative layers according to a geometric series, together with the condition that both the layers within each residual block are based on the same value of the scale parameter, which can be expressed as

$$\sigma_k = r^{k-1} \sigma_0, \quad (29)$$

where $r > 1$ represents the ratio between the scale parameters between adjacent scale levels.

This choice is similar to the construction of regular Gaussian derivative networks in Lindeberg (2022), and is also motivated by the further findings in Perzanowski and Lindeberg (2025c), where such a logarithmic distribution of the scale levels was empirically demonstrated to perform very well compared to a more general approach of learning the scale levels from training data.

Thus, given any input image $f: \mathbb{R}^D \rightarrow \mathbb{R}$, we have for the first Gaussian derivative layer with $k = \kappa = 1$

$$F_1^{\text{c}_{\text{out}}}(\cdot; \sigma_1) = \text{ReLU} \left(\text{BN} \left(\sum_{c_{\text{in}} \in [1, N_0]} \mathcal{J}_{\sigma_1}^{1, c_{\text{out}}, c_{\text{in}}} (f^{c_{\text{in}}}(\cdot)) \right) \right), \quad (30)$$

where

- the function BN denotes the batch normalisation operation,

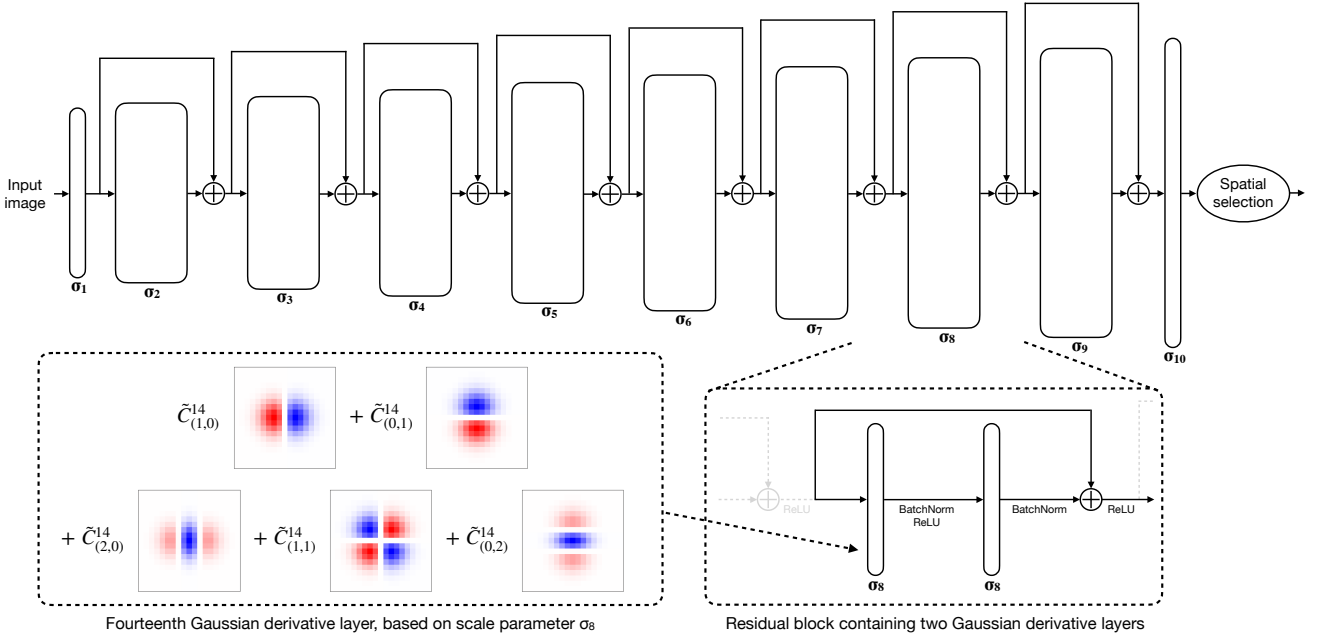


Fig. 3: Illustration of a single-scale-channel Gaussian derivative residual network consisting of 18 Gaussian derivative layers, together with the internal structure of a representative residual block, as well as an inside look into the composition of a Gaussian derivative layer within this residual block. The top part of the diagram illustrates the architecture of a single-scale-channel GaussDerResNet, with the layers organised into residual blocks, with the exception of the first and the last layers, which are regular Gaussian derivative layers. Each residual block is constructed out of two Gaussian derivative layers together with a skip connection, as defined in Equation (32), and shown in detail for the residual block \mathcal{M}_{σ_8} in the bottom right of the diagram, with the light grey dotted lines not part of the residual block and shown only for context. Whenever the sizes of the input or output feature channels do not match for a residual block, a standard projection is performed, involving using a 1×1 convolution (not depicted here) to match the dimensions of the residual signal. The single-scale-channel GaussDerResNet itself is parametrised by an initial scale value σ_0 , with the scale parameter of each layer determined according to a geometric distribution defined according to Equation (29), resulting in the sizes of the receptive fields increasing with the network depth, with each residual block using the same scale parameter value for both of its layers. Furthermore, each Gaussian derivative layer in the network consists of a convolution with a linear combination of discretised Gaussian derivative basis kernels $w(x; \sigma)$, as visualised in the bottom left of the diagram for layer $\kappa = 14$, where in the top row we see the contributions from the first order Gaussian derivatives, and in the bottom row the contributions from the second order Gaussian derivatives. Each basis kernel in the layer is computed by applying a corresponding central difference operator to a discrete analogue of Gaussian kernel defined with a corresponding scale parameter σ , as defined by Equation (59), while $\tilde{C}_\alpha = m(\alpha) C_\alpha \sigma^{|\alpha|}$ represents the learned weights of the layer, with the tilde symbol over the weight parameter C_α representing the corresponding scale normalisation factor $\sigma^{|\alpha|}$ and the multinomial normalisation factor $m(\alpha)$, both defined according to Equations (3) and (55). Finally, the output of the single-scale-channel GaussDerResNet is obtained by applying a spatial selection stage to the output of the final layer. The entire architecture is formally expressed in Equation (37).

- $f^{c_{\text{in}}}(\cdot)$ denotes the colour channel with index $c_{\text{in}} \in \{1, 2, 3\}$ for the case of colour input data,
- \mathcal{J}_{σ_1} denotes the operator for computing a Gaussian derivative layer at scale σ_1 corresponding to an extension of the definition

$$J(x; \sigma) = (\mathcal{J}_\sigma f)(x; \sigma) = (w(\cdot; \sigma) * f(\cdot))(x), \quad (31)$$

- w denotes the weights of the Gaussian derivative layer,
- c_{in} is the index for the input channels, and
- c_{out} is the index for the output channels.

For the intermediate layers, given an extension of the definition of the operator \mathcal{M}_σ for defining a residual

block at scale σ according to (18) to the form $\mathcal{M}_\sigma^{k, c_{\text{out}}, c_{\text{in}}}$ in the effective layer k in the network, a residual block in the GaussDerResNet is formally defined as

$$(\mathcal{M}_{\sigma_k} f)(x; \sigma_k) = \text{ReLU}(f(x) + \text{BN}((w_{\kappa+1}(\cdot; \sigma_k) * \text{ReLU}(\text{BN}((w_\kappa(\cdot; \sigma_k) * f(\cdot))))(x))), \quad (32)$$

where the layer indices κ are related to the effective layer indices k according to Equation (28). Thus, we can then formally define the successive residual blocks of a single-scale-channel GaussDerResNet in a recursive

manner as

$$F_{k+1}^{c_{\text{out}}}(\cdot; \sigma_{k+1}) = \sum_{c_{\text{in}} \in [1, N_k]} \mathcal{M}_{\sigma_{k+1}}^{k+1, c_{\text{out}}, c_{\text{in}}}(F_k^{c_{\text{in}}}(\cdot; \sigma_k)), \quad (33)$$

which can be written explicitly as

$$F_{k+1}^{c_{\text{out}}}(\cdot; \sigma_{k+1}) = \text{ReLU} \left(F_k^{c_{\text{in}}}(\cdot; \sigma_k) + \text{BN} \left(\sum_{c_{\mu} \in [1, N_k]} \mathcal{J}_{\sigma_{k+1}}^{\kappa+1, c_{\text{out}}, c_{\mu}} \left(\text{ReLU} \left(\text{BN} \left(\sum_{c_{\text{in}} \in [1, N_k]} \mathcal{J}_{\sigma_{k+1}}^{\kappa, c_{\mu}, c_{\text{in}}}(F_k^{c_{\text{in}}}(\cdot; \sigma_k)) \right) \right) \right) \right) \right), \quad (34)$$

where the intermediate feature channel index c_{μ} is typically set to $c_{\mu} = c_{\text{in}}$, and in the case when the feature channels c_{in} and c_{out} do not match, a 1×1 convolution based projection is applied to the skip connection, together with a batch normalisation stage, to match its feature dimension with the output. Note that the different indexing of the two Gaussian derivative layers reflects the fact that they use different weights, and similarly to the definitions for the Gaussian derivative layers, the bias terms are not explicitly shown.

Finally, for the last Gaussian derivative layer, we have that for a network with K layers, with Z denoting the number of effective layers computed by setting $\kappa = K$ in Equation (28):

$$F_{\text{final}}^c(\cdot; \sigma_Z) = F_Z^c(\cdot; \sigma_Z) = \text{ReLU} \left(\sum_{c_{\text{in}} \in [1, N_{Z-1}]} \mathcal{J}_{\sigma_Z}^{K, c, c_{\text{in}}}(F_{Z-1}^{c_{\text{in}}}(\cdot; \sigma_{Z-1})) \right), \quad (35)$$

where the corresponding output feature channel size c is defined to be equal to the number of possible classes, and F_{final} denotes the output of the final layer.

Because of the recursive definitions of the output of each successive layer or block defined above, which assume that the input at each level has been processed by the entire previous cascade in the hierarchy of the network, we introduce the notation A_{σ_0} to represent the output of the entire convolutional stage of the network

$$A_{\sigma_{i,0}}^c(f(\cdot)) = F_{\text{final}}^c(\cdot; \sigma_Z), \quad (36)$$

which is equivalent to the output of the final layer F_{final} defined in Equation (35). We will use both of these expressions interchangeably, as this is helpful for the mathematical notation in later definitions. The notation A is used when we want to make it clearer that the

output of the final layer depends on the input image f and the outputs of the previous stages in the cascade, and essentially represents all the 18 convolutional layers in the network.

To preserve the scale covariance and the scale invariance properties of the GaussDerResNets, the design of the scale channels does not contain any spatial subsampling operations.

3.4 Spatial selection mechanisms

In addition to the above pure primitive filtering stages, we also complement the GaussDerResNet architecture with explicit selection mechanisms over image space.

The final processing step in a single-scale-channel GaussDerResNet is a spatial selection stage, denoted as $\text{SpatSel}()$, which acts on the output tensor of the final convolutional layer, defined in Equation (36), by extracting a single value from each feature map, meaning one activation per class. Incorporating this operation into the architecture makes it possible to apply the GaussDerResNets to image classification tasks structurally similar to object recognition.

With this spatial selection mechanism in mind, a scale channel $\Gamma_{\sigma_0}: V \rightarrow \mathbb{R}^{N_Z}$ can now be defined, for a given input image $f \in V$, as the mapping

$$\Gamma_{\sigma_0}(f(\cdot)) = \text{SpatSel}(A_{\sigma_0}(f(\cdot))), \quad (37)$$

consisting of a convolutional stage and a spatial selection stage.

In this work, we consider two types of spatial selection operators $\text{SpatSel}()$: (i) central pixel extraction and (ii) spatial max pooling. Central pixel extraction, which is used to handle image data where the objects are *a priori* known to be centred, is defined as

$$\text{SpatSel}_{\text{centre}}(A_{\sigma_0}^c(f(\cdot))) = F_{\text{final}}^c(x_{\text{centre}}; \sigma_Z). \quad (38)$$

where c is the class index, and $x_{\text{centre}} = (x_1^{\text{centre}}, x_2^{\text{centre}}, \dots, x_D^{\text{centre}})^T$ refers to the pixel position in the centre of the final output feature map. For discrete image data, in the case of an even input signal size, the central extraction step is approximated as an average of the central $2 \times 2 \times \dots \times 2$ pixel region in the image.

Spatial max pooling is introduced to handle datasets with non-centred objects

$$\text{SpatSel}_{\text{spat-max}}(A_{\sigma_0}^c(f(x))) = \max_x F_{\text{final}}^c(x; \sigma_Z), \quad (39)$$

and implies the selection of the response from the image position, where the response to a particular effective feature detector is as its strongest. This region-of-interest mechanism is structurally similar to the way

spatial extrema of differential entities are used in classical differential feature extractors and interest point detectors, see Lindeberg (1998b; 2015) for more details.

3.5 Scale covariance properties of Gaussian derivative residual networks

Covariant deep networks² have built in prior knowledge about how to handle certain symmetries in the data, making their outputs more interpretable and theoretically well defined, which in turn makes their behaviour more predictable. Additionally, during training, the network capacity is not spent on learning given symmetries in the data, since the ability to handle these symmetries has already been hard-coded into the architecture. This is particularly useful when large datasets containing sufficient variabilities in the data are not available. Furthermore, incorporating priors about spatial scaling transformations makes it possible for the resulting scale covariant networks to perform scale generalisation, to process image data at scales that are not spanned by the training data.

Formally, given a group action \mathcal{S} of the scaling group, consisting of uniform scaling transformations of the form

$$f' = \mathcal{S}_s f, \quad (40)$$

scale covariance of an operator Φ applied to an input function f can be defined as the commutation relation:

$$\Phi'(\mathcal{S}_s f) = \mathcal{S}_s \Phi(f) \quad \forall s \in \mathcal{S}, f \in \Omega, \quad (41)$$

where Φ' is either the same operator as Φ or some sufficiently closely related operator, such as a constant multiplied by Φ . In general, an operator is said to be covariant with respect to a family of transformations that form a group, if it commutes with the action of every transformation in the family. This means that if the input f is transformed by a group action, the output should be transformed in a corresponding manner.

Given such a definition of covariance, the GaussDerResNet architecture is manifestly scale covariant, which follows directly from the scale matching properties derived in Section 3.1, which can be chained in cascade, layer by layer, thus enabling scale matching between corresponding layers in the scale channels. Figure 4 shows a commutative diagram that illustrates

² In some literature, the terminology “equivariant deep networks” is also used. In this treatment, we use terminology “covariant” to be consistent with the terminology in classical scale-space theory (Lindeberg 2013b), reflecting the property that the image representations “co vary” with the geometric image transformations, without not necessarily varying in an exactly equal manner, for example, differing in some smaller respect, such as a rescaling of the amplitude of the response.

these chained scale covariance properties in all the layers in a GaussDerResNet. This property enables the network to process uniformly scaled image data in a theoretically well-defined way, by ensuring that the output transforms in a predictable and desirable manner under spatial scaling transformations.

3.6 Multi-scale-channel Gaussian derivative residual networks with scale selection by pooling over scales

A scale-invariant GaussDerResNet can be constructed by gathering a set of scale channels together in parallel, and combining their output through a permutation-invariant pooling stage. Such an architecture is referred to as a multi-scale-channel GaussDerResNet. In such a network, all the scale channels I are copies of each other, meaning they share the same weights and are parametrised by the same relative scale ratio r between the adjacent scale channels. The only difference between these scale channels is that they are based on different initial scale values, with the i :th scale channel based on $\sigma_{i,0}$, with all the scale parameters in the deeper layers matched accordingly, according to Equation (29). This means that the receptive field sizes of the Gaussian derivative basis kernels in each layer of a scale channel steadily increase, proportional to the initial scale value of the scale channel. The i :th scale channel is therefore denoted as $I_{\sigma_{i,0}}$.

Similarly to Equation (29), we also choose the initial scale levels $\sigma_{n,0} \in \mathbb{R}_+$ in the multi-scale-channel networks according to a geometric distribution

$$\sigma_{n,0} = \lambda^{(n-1)} \cdot \sigma_{1,0}, \quad (42)$$

where $\lambda \in \{\sqrt{2}, \sqrt[4]{2}\}$ is the ratio between the initial scale levels between adjacent scale channels.

Scale invariance of the multi-scale-channel network is achieved by using a permutation-invariant pooling stage over the scale channels for classification, instead of a fully connected classification layer. This pooling operation over scales, denoted as $\text{ScaleSel}()$, acts as selection mechanism over the set of scale channels. Similar to the expression in Equation (37) for a single-scale-channel GaussDerResNet, we can therefore define the entire multi-scale-channel GaussDerResNet with N scale channels as

$$\text{Prediction} = \text{ScaleSel}(\{I_{\sigma_{i,0}}(f(\cdot))\}_{i=1}^N), \quad (43)$$

where the corresponding class channel of the prediction, that is maximally activated, is selected as the final classification. In this work, we consider three possible types

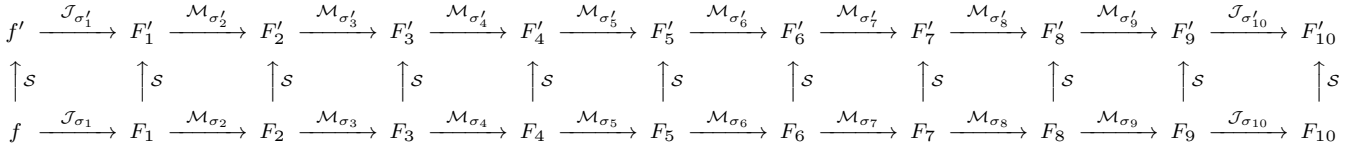


Fig. 4: Commutative diagram for the entire 18-layer Gaussian derivative residual network, illustrating the scale-covariant properties of the architecture. In the diagram, $\mathcal{J}_{\sigma'_i}$ represents a Gaussian derivative layer at the scale σ'_i , $\mathcal{M}_{\sigma'_i}$ represents a Gaussian derivative residual block at the scale σ'_i , and both are based on Gaussian derivative primitives up to a given order ν of spatial differentiation. The scaling operator \mathcal{S} acts on both the image domains and the scale parameters (of the input image f or the layer and residual block outputs F_i), representing a uniform scaling transformation $(x'; \sigma') = (Sx; S\sigma)$ with a scaling factor $S \in \mathbb{R}_+$. The commutative diagram should be read from the bottom left to the top right, and shows that each level in the cascade of the network can be matched under arbitrary scaling transformations \mathcal{S} according to $F_i^{c_{\text{out}}}(x; \sigma_i) = F_i^{c_{\text{out}}}(Sx; S\sigma_i)$, provided that such matching has also been done in the same manner at every previous step in the hierarchy, including the input image. As described in Section 3.1, these scale covariance properties are not affected by the use of residual connections, or the presence of batch normalisation or non-linear ReLU stages in the network.

of permutation-invariant pooling over scale channels.³ These include:

- *max pooling* over scales F_{max}^c , defined as

$$\begin{aligned} \text{ScaleSel}_{\text{max}}(\{F_{\sigma_{i,0}}^c(f(\cdot))\}_{i=1}^N) &= \\ &= F_{\text{max}}^c = \max_{i \in \{1, 2, \dots, N\}} \text{SpatSel}(A_{\sigma_{i,0}}^c(f(\cdot))), \end{aligned} \quad (44)$$

- *logsumexp pooling* (a smooth approximation to the maximum) over scales $F_{\text{logsumexp}}^c$, defined as

$$\begin{aligned} \text{ScaleSel}_{\text{logsumexp}}(\{F_{\sigma_{i,0}}^c(f(\cdot))\}_{i=1}^N) &= \\ &= F_{\text{logsumexp}}^c = \log \sum_{i=1}^N \exp(\text{SpatSel}(A_{\sigma_{i,0}}^c(f(\cdot)))) \end{aligned} \quad (45)$$

- and *average pooling* over scales F_{average}^c , defined as

$$\begin{aligned} \text{ScaleSel}_{\text{average}}(\{F_{\sigma_{i,0}}^c(f(\cdot))\}_{i=1}^N) &= \\ &= F_{\text{average}}^c = \frac{1}{N} \sum_{i=1}^N \text{SpatSel}(A_{\sigma_{i,0}}^c(f(\cdot))), \end{aligned} \quad (46)$$

given any input image f and any class index c .

Notably, these constructions bear close similarities to how scale selection mechanisms are constructed in classical computer vision, see Lindeberg (1998b, 1998a,

2013c, 2015, 2021b). Specifically, the combination of spatial max pooling with max pooling over scales can be seen as a generalisation of the notion of scale-space extrema in Lindeberg (1998b, 2015) and Lowe (2004). Average pooling over scale can also be seen as a generalisation of the notion of scale selection by weighted averaging over scales in Lindeberg (2013c, 2015).

The entire multi-scale-channel GaussDerResNet architecture is illustrated in Figure 5. This network is provably scale covariant and scale invariant. Experimentally, we will demonstrate that the network is capable of scale generalisation, meaning that it can achieve high performance even when tested at scales not encountered during training. The range of scales, that this model is able to handle, is determined by the scale range spanned by the initial scale values $\sigma_{i,0}$ of the scale channels. Due to the weight sharing, each scale channel is responsible for handling a single scale level corresponding to its initial scale level $\sigma_{i,0}$, meaning that if an image featuring a pattern, that has been learned during training, is rescaled and then provided as input, then the scale channel at a matching scale level will be strongly activated in response to it, even if the given scale level has not been previously seen during training.

Additionally, with a dense enough distribution of the initial scale levels $\sigma_{i,0}$, as defined according to Equation (42), the multi-scale-channel GaussDerResNet can automatically compute good approximations to smooth interpolation between the scales in between the scale channels, resulting in a flat and smooth scale generalisation curve across the entire operational scale interval. This means that neighbouring scale channels can approximately cover the entire in-between scale range, due to the discretised nature of the filter in the Gaussian derivative layers and the scale selection properties of the network, effectively allowing for scale-invariant

³ In the deep learning literature, residual convolutional networks often make use of a fully connected layer for classification. Such an architectural choice is, however, avoided in our GaussDerResNets, since it would combine information from different spatial points, which would then break the scale covariance. Alternatively, a linear layer could be used in GaussDerResNets after the spatial selection stage, which would not break the scale covariance. In this work, we do, however, not make use of any last linear layer, since we have not found such a layer to improve the performance.

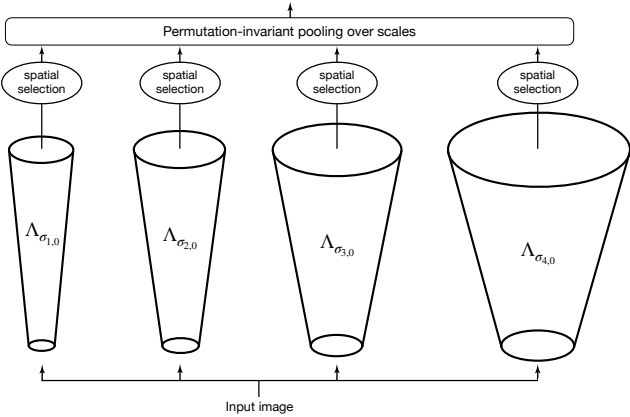


Fig. 5: Conceptual illustration of a multi-scale-channel GaussDerResNet, composed of 4 parallel single-scale-channel GaussDerResNets, referred to as scale channels. Each scale channel is constructed as shown in the top part of Figure 3, and the i :th scale channel denoted as $\Gamma_{\sigma_{i,0}}$, defined in Equation (37), consisting of the (i) convolutional stage $\Lambda_{\sigma_{i,0}}$, composed of 18 Gaussian derivative layers, represented by the conical frustums (meaning the tapered cylinders) in the diagram, indicating the increase of receptive field size with depth, and (ii) the spatial selection stage. There is a geometric distribution of the spacing between the initial scale values $\sigma_{i,0}$, that the scale channels are based on, set by a fixed ratio, as expressed in Equation (42). Each scale channel processes a copy of the input image, and crucially, in order to achieve scale covariance, the scale channels share the same weights, with all the scale channels parametrised by the same relative scale ratio r . Finally, instead of a fully connected classification layer, permutation-invariant pooling over the scale channels is performed as a final processing stage in the network. The entire architecture is formally expressed in Equation (43).

processing, despite using only a finite amount of scale channels when implemented in the real-world setting.

Finally, we also include *boundary* scale channels at both the ends of the scale interval to reduce the possible artefacts that could otherwise occur due to image structures falling outside the operational scale range.

3.7 Scale invariant property of Gaussian derivative ResNets with scale selection mechanisms for image classification

The scale invariance of the multi-scale-channel GaussDerResNet architecture can be mathematically proven, following arguments similar to those presented in Lindberg (2022), given the assumptions that the Gaussian derivative basis filters are continuous and the network is constructed out of an infinite number of scale channels. Here, we present a proof for the more general D -dimensional case, with the multi-scale-channel GaussDerResNet based on any permutation invariant scale

pooling mechanism. Furthermore, we consider a setup where the spatial selection mechanism in a GaussDerResNet is performed using spatial max pooling, meaning that the maximum value over scales can be selected at any spatial location within the image, making the output translation covariant.

A scale invariant deep network is a vision system with an inherent ability to classify objects of *a priori* unknown size, where the learned features can be recognised and treated in the same way at any scale. In general, scale invariance is a form of inductive bias, that enables deep networks to have good scale generalisation properties, meaning the ability to perform well on scales not seen during training, thereby eliminating the need to learn how to handle different scales directly from data.

Using the notation of Section 3.5, scale invariance can formally be defined as

$$\Phi(\mathcal{S}_s f) = \Phi(f) \quad \forall s \in \mathcal{S}, f \in \Omega, \quad (47)$$

making it a stronger condition/criterion than that of scale covariance defined in Equation (41), since now applying a group action of the scaling group to the input is equivalent to applying the identity transformation.

Proving scale invariance of multi-scale-channel GaussDerResNets based on spatial max pooling amounts to showing that

$$\begin{aligned} \text{SpatSel}_{\text{spat-max}}(\Lambda_{\sigma'_0}^c(f'(x'))) &= \\ &= \text{SpatSel}_{\text{spat-max}}(\Lambda_{\sigma_0}^c(f(x))), \end{aligned} \quad (48)$$

under the spatial scaling transformation $f'(x') = f(x)$ for $x' = Sx$, with the scale parameters transformed according to $\sigma' = S\sigma$.

In the continuous case, the network is based on an infinite set of scale channels with shared weights, with their initial scale values σ_0 taking all the possible values in \mathbb{R}_+ . When a (uniform) spatial scaling transformation is performed around the point x_{origin}^D , we find that, given Equations (13) and (14), and using the notation from Equation (43) that:

$$\{\Gamma_{\sigma_{i,0}}(f(x))\}_{i=1}^{\infty} = \{\Gamma_{\sigma'_{i,0}}(f'(x'))\}_{i=1}^{\infty}. \quad (49)$$

This equality implies that the application of any permutation invariant scale selection operator $\text{ScaleSel}()$ to either side of Equation (49) results in the same output, proving scale invariance of the architecture.

When the entire network is discretised over space and along the scale direction, with the initial scale values $\sigma_{i,0}$ distributed in a self-similar manner, these continuous properties will be approximated numerically, assuming that we have a sufficiently dense distribution of the scale levels, and based on the assumption

that the discrete Gaussian kernels constitute sufficiently good numerical approximations of the underlying continuous Gaussian kernels. In practice, the latter numerical approximation property will be more accurate at coarser spatial scales than at finer spatial scales.

The key role of using the spatial max pooling operation in GaussDerResNets is that it ensures the translation covariance properties within these networks, as it facilitates the feature maps to be shifted proportionally to the shift in the input. In fact, the output of each scale channel shifts proportionally to the shift in the input, by a factor corresponding to the given scale levels in the scale channels. In general, this guarantees that scale invariance will approximately hold for all image positions that are sufficiently far away from the image boundary. In the ideal continuous case with an infinite image domain, it holds that the scale-space maxima translate with the translation of the input, given an image transformation consisting of a scaling \mathcal{S} followed by a translation: $x' = \mathcal{S}(x - x_1) + x_2$, with $x_1 = x_0$ and the spatial shift component given by $x_2 = x_0 + \Delta x$, where $\Delta x \in \mathbb{R}^D$.

3.8 Additional extensions regarding design options

In addition to the above general architecture for GaussDerNets, we will also consider a few modifications:

3.8.1 The use of a zero-order term in the Gaussian derivative residual layers

In the original formulation of GaussDerNets in Lindeberg (2022), the linear combinations of Gaussian derivative responses was performed for strictly positive orders of differentiation, motivated by the theoretically desirable property of having the responses in the deep network being unaffected by intensity transformations of the form $f(x) \mapsto f(x) + a$ for any constant $a \in \mathbb{R}$, which model local multiplicative illumination transformations on a logarithmic intensity scale, see Lindeberg (2013a) Section 2.3 for a more extensive treatment. Therefore, the use of a term in the Gaussian derivative layer that depends on the zero-order Gaussian smoothed image information was excluded, since such a term would depend on the absolute value of the image intensity and not just on relative differences in intensity.

Given that the first layer in the GaussDerResNet has been computed using only strictly positive orders of spatial differentiation, one could, however, conceive including the zero-order terms in the higher layers.⁴ This

⁴ In the deep learning literature, most other networks, that parametrise their receptive fields using the N-jet Gaussian

corresponds to extending the set of Gaussian derivative responses for a second-order Gaussian derivative residual layer in the higher layers (3) according to (6) to

$$\alpha \in \{(0, 0), (1, 0), (0, 1), (2, 0), (1, 1), (0, 2)\}. \quad (50)$$

and extending the set of Gaussian derivative responses for a third-order Gaussian derivative residual layer in the higher layers according to (7) to

$$\alpha \in \{(0, 0), (1, 0), (0, 1), (2, 0), (1, 1), (0, 2), \dots, (3, 0), (2, 1), (1, 2), (0, 3)\}. \quad (51)$$

In Section 7.1, we will compare these two approaches for defining the higher layers in the GaussDerResNets.

3.8.2 Depthwise-separable Gaussian derivative residual networks

Work by Chollet (2017) and Howard *et al.* (2017), with continued work on ConvNeXt by Liu *et al.* (2022) and Woo *et al.* (2023), has demonstrated that the amount of computational work in deep networks can be substantially decreased, by decoupling the convolution operations across the layers from the spatial convolutions.

For the GaussDerResNet architecture described in Section 3.3, this corresponds to replacing the operation for computing the next layer from the previous layer for the simplest form of a residual block of the form (8)

$$\begin{aligned} F_{k+1}^{\text{c}_{\text{out}}}(\cdot; \sigma_{k+1}) &= \sum_{c_{\text{in}} \in [1, N_k]} \mathcal{M}_{\sigma_{k+1}}^{k+1, c_{\text{out}}, c_{\text{in}}}(F_k^{\text{c}_{\text{in}}}(\cdot; \sigma_k)) = \\ &= \text{ReLU} \left(F_k^{\text{c}_{\text{in}}}(\cdot; \sigma_k) + \right. \\ &\quad \left. + \sum_{c_{\text{in}} \in [1, N_k]} w^{k+1, c_{\text{out}}, c_{\text{in}}}(\cdot; \sigma_{k+1}) * F_k^{\text{c}_{\text{in}}}(\cdot; \sigma_k) \right) \end{aligned} \quad (52)$$

to instead applying a two-stage computation of the form

$$\begin{aligned} F_{k+1}^{\text{c}_{\text{out}}}(\cdot; \sigma_{k+1}) &= \sum_{c_{\text{in}} \in [1, N_k]} \mathcal{N}_{\sigma_{k+1}}^{k+1, c_{\text{out}}, c_{\text{in}}}(F_k^{\text{c}_{\text{in}}}(\cdot; \sigma_k)) = \\ &= \text{ReLU} \left(F_k^{\text{c}_{\text{in}}}(\cdot; \sigma_k) + \right. \\ &\quad \left. + \sum_{c_{\text{in}} \in [1, N_k]} \alpha^{k+1, c_{\text{out}}, c_{\text{in}}} h^{k+1, c_{\text{in}}}(\cdot; \sigma_{k+1}) \right) \end{aligned} \quad (53)$$

derivative basis, typically include a zero-order term in all the layers, see, e.g., Jacobsen *et al.* (2016) and Pintea *et al.* (2021).

for some set of scalar weights $\alpha^{k+1, c_{\text{out}}, c_{\text{in}}} \in \mathbb{R}$ that are to be learned, where the intermediate functions $h^{k, c_{\text{in}}} : \mathbb{R}^D \times \mathbb{R} \rightarrow \mathbb{R}$ are defined according to

$$h^{k+1, c_{\text{in}}}(x; \sigma_{k+1}) = (w^{k+1, c_{\text{in}}}(\cdot; \sigma_{k+1}) * F_k^{c_{\text{in}}}(\cdot; \sigma_k))(x) \quad (54)$$

for some set of filter weight functions $w^{k+1, c_{\text{in}}} : \mathbb{R}^D \times \mathbb{R}_+ \rightarrow \mathbb{R}$, that may be either specified *a priori* or be learned.

In this way, the computational work needed to perform the spatial convolutions can be reused when computing the different output in the different channels of the next layer, thereby substantially decreasing the amount of computations. In this work, we will specifically consider linear combinations of Gaussian derivative operators of the form (3)

$$w^{k+1, c_{\text{in}}}(x; \sigma) = \sum_{\alpha: |\alpha| \leq N} m(\alpha) C_{\alpha}^{k+1, c_{\text{in}}} \sigma^{|\alpha|} g_{x^{\alpha}}(x; \sigma), \quad (55)$$

where the coefficients $C_{\alpha}^{k+1, c_{\text{in}}}$ are to be learned.

3.9 Discrete implementation of Gaussian derivative residual networks

As the default method for discrete implementation of the Gaussian derivative operators, we first use separable convolution along each dimension with the discrete analogue of the Gaussian kernel (Lindeberg 1990)

$$T(n; \sigma) = e^{-s} I_n(s), \quad (56)$$

for $s = \sigma^2$, where I_n denotes the modified Bessel functions of integer order n (Abramowitz and Stegun, 1964). Then, we apply central difference operators of the forms

$$\delta_x = (-1/2, 0, 1/2), \quad (57)$$

$$\delta_{xx} = (1, -2, 1), \quad (58)$$

to the spatially smoothed image data, implying that any Gaussian derivative operator $g_{x^{\alpha}}$ of order $\alpha = (\alpha_1, \alpha_2, \dots, \alpha_D)$ will be approximated by

$$g_{x^{\alpha}}(\cdot; \sigma) = g_{x_1^{\alpha_1} x_2^{\alpha_2} \dots x_D^{\alpha_D}}(\cdot; \sigma) \approx \delta_{x_1^{\alpha_1}} \delta_{x_2^{\alpha_2}} \dots \delta_{x_D^{\alpha_D}} T_1(\cdot; \sigma) T_2(\cdot; \sigma) \dots T_D(\cdot; \sigma), \quad (59)$$

where $T_i(\cdot; \sigma)$ denotes the 1-D discrete analogue of the Gaussian kernel according to (56) along the i :th coordinate direction, and $\delta_{x_i^{\alpha_i}}$ denotes the composed difference operator of order α_i along the i :th coordinate direction defined by

$$\delta_{x_i^{\alpha_i}} = \begin{cases} \delta_{x_i x_i}^j & \text{if } \alpha_i = 2j, \\ \delta_{x_i} \delta_{x_i x_i}^j & \text{if } \alpha_i = 2j + 1, \end{cases} \quad (60)$$

for integer j , where δ_{x_i} denotes the first-order central difference operator according to (57) along the i :th coordinate direction and $\delta_{x_i x_i}$ denotes the second-order central difference operator according to (58) along the same direction.

The motivation for this choice is that this method has in Lindeberg (2024; 2025a) and Perzanowski and Lindeberg (2025c) been demonstrated to constitute the best choice among a larger set of discrete approximations in terms of (i) sampled Gaussian derivative kernels, (ii) integrated Gaussian derivative kernels or (iii) convolution with the normalised sampled Gaussian kernel complemented with central differences or (iv) convolution with the integrated Gaussian kernel complemented with central differences. Specifically, by the use of multiple small support central difference operators for each order of spatial differentiation, the spatial smoothing operation can be *shared* between the receptive fields for the different orders of spatial differentiation in the Gaussian derivative residual layers, thereby increasing the computational efficiency.

4 Datasets

For evaluating the proposed GaussDerResNets experimentally, we will consider two main types of use cases:

- computing the accuracy of single-scale-channel GaussDerResNets on the regular STL-10 dataset, and
- characterising the scale generalisation performance of multi-scale-channel GaussDerResNets on the previously existing Rescaled Fashion-MNIST and Rescaled CIFAR-10 datasets (Perzanowski and Lindeberg 2025c) as well as on the here newly created Rescaled STL-10 dataset.

4.1 Rescaled image datasets

To assess the ability of the GaussDerResNets to generalise to scales not present in the training data, we evaluate them on three rescaled image datasets, which contain spatial scaling variations up to a factor of 4 in the corresponding test datasets. In this study, we first investigate the scale generalisation properties of networks on the rescaled Fashion-MNIST and the rescaled CIFAR-10 datasets. To evaluate the scale generalisation properties of networks on relatively higher resolution natural image data, we also introduce and investigate the rescaled STL-10 dataset.

All the three rescaled datasets have been created using the same design philosophy, where the images in the training datasets remain at the original size, referred to

as the size factor 1, while multiple copies of the test set are created, with each copy rescaled by a single size factor. The goal is to train the networks on images of the original size, and then evaluate them on identical sets of test datasets, that each have the images rescaled by a certain single size factor. For each rescaled dataset, the possible test dataset image scaling factors S that are considered are

$$S \in \{1/2, 2^{-\frac{3}{4}}, 2^{-\frac{2}{4}}, 2^{-\frac{1}{4}}, 1, 2^{\frac{1}{4}}, 2^{\frac{2}{4}}, 2^{\frac{3}{4}}, 2\}, \quad (61)$$

which are within the range of interest $[1/2, 2]$, each separated by a relative scaling factor of $\sqrt[4]{2}$.

4.1.1 The rescaled Fashion-MNIST dataset

The rescaled Fashion-MNIST dataset⁵ (Perzanowski and Lindeberg 2025c), was created by extending the Fashion-MNIST dataset (Xiao et al. 2017) with spatial scaling variations in the test dataset, for size factors according to Equation (61). The dataset contains 72×72 grayscale images of clothing items, belonging to 10 different classes. Each sample depicts a clothing item centred in the frame, with a completely black background. The dataset comprises a total of 70 000 images, partitioned into 50 000 training samples, 10 000 validation samples, and 10 000 test samples.

4.1.2 The rescaled CIFAR-10 dataset

The rescaled CIFAR-10 dataset⁶ (Perzanowski and Lindeberg 2025c), was created by extending the CIFAR-10 dataset (Krizhevsky and Hinton 2009) with spatial scaling variations in the test dataset, for size factors given by Equation (61). The dataset contains 64×64 RGB images of real-world photographs of animals or vehicles, belonging to 10 different classes, with the object in each sample being centred in the frame. In order to have all the training and the test images at the same resolution, mirror extension is used to extend the images to size 64×64 for scaling factors less than 2. The dataset comprises a total of 60 000 images, partitioned into 40 000 training samples, 10 000 validation samples, and 10 000 test samples.

4.1.3 The rescaled STL-10 dataset

We introduce a modified version of the labelled subset of the STL-10 dataset (Coates et al. 2011), which is a subset of the ImageNet dataset, extended with scaling

variations, to allow for evaluating the scale generalisation properties of the model in more challenging natural settings, at a much higher pixel resolution than in the CIFAR-10 dataset.

The original labelled subset of the STL-10 dataset, with 5 000 training samples and 8 000 test samples, consists of real-world 96×96 RGB images of vehicles and animals from the 10 distinct classes: “airplane”, “bird”, “car”, “cat”, “deer”, “dog”, “horse”, “monkey”, “ship” and “truck”, all of which, with the exception of the class “monkey”, are also present in the CIFAR-10 dataset. A semi-automated cleaning stage was performed prior to the rescaling of this dataset, to remove images for which mirroring at the image boundaries would have substantial negative effects. This cleaning stage mainly involved removing the artificial constant padding in some of the images. In addition, most blurry, poorly lit, severely off-centre or substantially obscured images were manually removed, to improve the quality of the dataset, resulting in about 10% of the original dataset being removed.

Just as for the rescaled Fashion-MNIST and CIFAR-10 datasets, bicubic interpolation with default anti-aliasing in Matlab was used for generating the scaled images, with the considered image size factors given by Equation (61). The training dataset still uses the original size factor 1, as well as the original image size of 96×96 pixels to keep training-time memory usage low, with mirror extension being used, to achieve the desired image size if de-padding was applied during the cleaning stage. Meanwhile, copies of the test dataset were created, each dedicated to one of the scaling factors S in Equation (61). The images in each test set were extended with mirroring at the boundaries to an image size of 192×192 pixels, meaning that the test sets use a larger image size compared to the training set, even at the size factor 1. See Figure 6 for an illustrative overview of example images from this dataset.

The dataset comprises a total of 11 600 images, partitioned into 7 000 training samples, 1 000 validation samples, and 3 600 test samples. The small size of this dataset also enables it to be used to evaluate the ability of networks to generalise from limited training data.

Note that the input images used for generating the rescaled STL-10 dataset also comprise a certain variability in the sizes of the objects in the image domain, due to factors such as the viewing distance or direction of the camera. Furthermore, in contrast to the CIFAR-10 dataset, the objects in the images are not always centred, with a greater amount of background typically included within the frame, as the images are less cropped. Thus, the scale selection properties may be less clear-cut for this dataset than for the rescaled Fashion-MNIST or CIFAR-10 datasets.

⁵ The rescaled Fashion-MNIST dataset is available for download at Zenodo, see Perzanowski and Lindeberg (2025b).

⁶ The rescaled CIFAR-10 dataset is available for download at Zenodo, see Perzanowski and Lindeberg (2025a).

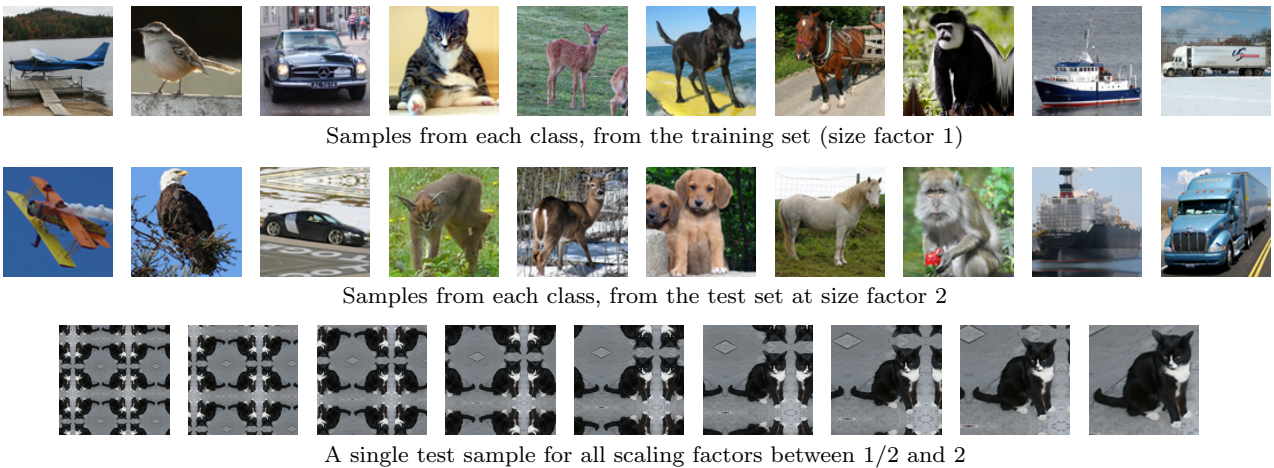


Fig. 6: A collage made up of a representative subset of images from the rescaled STL-10 dataset. The **(top row)** contains samples from the training set (size factor 1), each with 96×96 pixels (with the pixel size adapted to fit the collage), with one example per class, where the 10 classes are: “airplane”, “bird”, “car”, “cat”, “deer”, “dog”, “horse”, “monkey”, “ship” and “truck”. In a similar manner, the **(middle row)** depicts samples from the size factor 2 test set, each with 192×192 pixels. The **(bottom row)** depicts a single sample from the “cat” class in the test set, for each possible scaling factor between $1/2$ and 2, with the scaling factor increasing from left to right, and the images at all the size factors extended (if needed) using mirroring to the final image size of 192×192 pixels. Note that this means that the size factor 1 test set has mirror extensions and a larger image size compared to the training set.

Model Parameters	Symbol	rescaled Fashion-MNIST	rescaled CIFAR-10	rescaled STL-10
Number of scale channels	N	6	6	6
Initial scale value range	$[\sigma_{i,0}]$	$[\sqrt{2}^{-3}, 2]$	$[\sqrt{2}^{-3}, 2]$	$[\sqrt{2}^{-3}, 2]$
Relative scale ratio	r	1.13	1.2	1.32
Relative truncation error bound	ϵ	0.01	0.005	0.005
Number of layers	K	18	18	18
Intermediate feature channels	c	1-48-24-32-48-64-128-10	3-48-64-192-256-10	3-48-64-128-192-256-10
Spatial selection method	-	central pixel	central pixel	spatial max pooling
Zeroth-order term	-	without	without	with
Number of network parameters	-	295k	1.78M	2.07M
Input image size	-	$1 \times 72 \times 72$	$3 \times 64 \times 64$	$3 \times 96 \times 96$

Table 1: Key parameter values and mechanisms employed in our experiments with the multi-scale-channel GaussDerResNets, for the three rescaled datasets. In the row specifying the number of intermediate feature channels c , a line over a number means that two blocks in a row use the same value, while two lines means that three blocks in a row use the same value.

Training Parameters	rescaled Fashion-MNIST	rescaled CIFAR-10	rescaled STL-10
Number of training iterations (epochs)	30000 (32)	100000 (90)	56000 (119)
Batch size	64	45	17
Initial learning rate	0.01	0.01	0.01
Number of warm-up epochs	0	8	8
Weight decay	0.025	0.025	0.025
Scale channel dropout factor	0.2	0.3	0.3
Random cropping	none	none	yes (padding=24)

Table 2: Training configurations for multi-scale-channel GaussDerResNet employed in our experiments, for the three rescaled datasets.

5 Network architectures and training configurations

This section describes the network architecture and the training parameters used to evaluate the GaussDerResNets and their variants on the rescaled datasets introduced in Section 4.1. For each dataset, we used the

predefined data splits, employing the validation sets to select the hyperparameter settings and the training schedule.

5.1 Network architecture design

The architectural specifications for the multi-scale-channel Gaussian derivative residual networks (GaussDerResNets) were chosen through model selection, to achieve strong scale generalisation properties and performance on the considered rescaled datasets, and are summarised in Table 1. The GaussDerResNet design is formally defined in Sections 3.3 and 3.6

The initial scale values $\sigma_{i,0}$ are the main network parameters that determine the range of size factors, not seen during training, that the network can generalise to. For the rescaled datasets used in this work, the possible scales are given by Equation (61), which is what motivates the choice of $\sigma_{i,0} \in \{1/(2\sqrt{2}), 1/2, 1/\sqrt{2}, 1, \sqrt{2}, 2\}$, to cover that range with an adequate spacing of $\sqrt{2}$, while also including an additional boundary scale channel for the smaller size factors, based on $\sigma_{i,0} = 1/(2\sqrt{2})$. The value of the relative scale factor r is chosen based on the original image size, with higher values picked for larger sizes.

The number of feature channels c used by each network, provided in Table 1, specifies the values for each effective layer, following Equation (28). The first and the last values represent the input colour channels and the number of output classes, respectively, while the intermediate values represent the input feature channel number in the intermediate residual blocks, with one value per block. In Table 1, when two residual blocks in a row use the same value, we denote that with a line over the number, and three residual blocks in a row with two lines over the number.

Before the permutation-invariant scale pooling stage, the GaussDerResNets and their variants explored in our experiments are configured to use a spatial selection mechanism that is based on either (i) central pixel extraction, or (ii) spatial max pooling. The chosen design depends on whether the objects within the frame of the images for a given dataset are centered or not. The possible approaches to permutation-invariant pooling over scales that we consider are either max pooling, logsum-exp pooling, or average pooling.

5.2 Training protocol

To train the GaussDerResNets and their variants on the rescaled datasets, we used the AdamW optimiser with the cross-entropy loss, with all the training settings summarised in Table 2. For all the datasets, the network weights were initialised using a uniform He initialisation. The batch size was selected per dataset based on network size, input resolution, and single-GPU memory limits; to maximise the model capacity. We

trained the largest feasible networks, which in the case of the rescaled STL-10 dataset required a small batch size due to memory constraints. The number of epochs was also dataset dependent, because the more complex datasets require longer training. Regarding the learning rate, a cosine decay schedule was used, with the learning rate decreasing from the initial value to 10^{-5} , over the course of the training epochs. Additionally, for the rescaled CIFAR-10 and STL-10 datasets, the learning rate was warmed up from 10% of its initial value to the full initial value over the first 8 epochs.

Since the selected training configurations have been found during the hyperparameter search, the training and the validation datasets were combined to maximize the available training data.

To enhance the generalisation ability of the networks and to prevent overfitting, several data augmentation and regularisation techniques were employed during training. Random horizontal flipping with a probability of 0.5 was used to enhance the sample diversity in the training set, while for the RGB datasets random colour jitter configured with the parameters (brightness=0.2, contrast=0.2, saturation=0.2, hue=0.05) was also used. Additionally, random cropping to original size after padding is used when training on the rescaled STL-10 dataset.

We also used scale-channel dropout, see Perzanowski and Lindeberg (2025c), which involves applying dropout across the outputs from the scale channels before the permutation-invariant scale pooling stage, which enables the network to make better use of the information across the different scales during training.

Additionally, we used label smoothing, unless specified otherwise, which is a regularisation technique that prevents overconfidence during classification, by replacing hard one-hot target labels with softened (smoothed) probability distributions during training. This improves generalisation and can help reduce overfitting, see Müller et. al (2019), which is important for achieving good scale generalisation. A smoothing parameter of 0.1 was used in all our experiments.

6 Experiments

In this section, we will evaluate the properties of the GaussDerResNet networks:

- regarding the accuracy of single-scale-channel GaussDerResNets on the regular STL-10 dataset in Section 6.1, and
- regarding the scale generalisation and the scale selection properties for multi-scale-channel GaussDerResNets applied on the Rescaled Fashion-MNIST,

the Rescaled CIFAR-10 and the Rescaled STL-10 datasets in Sections 6.2.1–6.2.3.

6.1 Experiments with single-scale-channel networks on the regular STL-10 dataset

The newly proposed Gaussian derivative residual network (GaussDerResNet) architecture is provably scale covariant and scale invariant, but also has greatly improved generalisation capabilities compared to the previously studied Gaussian derivative networks. To demonstrate that the single-scale-channel GaussDerResNet can achieve competitive performance on image classification tasks, we trained and evaluated the network on the labelled subset of the regular STL-10 dataset, and compared the results to several other well performing networks on this dataset.

The training was for the most part performed according to the procedure outlined in Section 5 for multi-scale-channel networks applied on the rescaled STL-10 dataset, with the main difference being that a single-scale-channel of the network based on $\sigma_0 = 0.5$ was used, and the relative scale ratio was set to $r = 1.5$. With the exception of the first layer, the network layers included a zero-order term, and spatial max pooling was used after the final layer as the spatial selection mechanism. Additional regularisation was performed during training by the use of random cropping and dropout.

In this comparison study, we considered two different variants of the GaussDerResNets, one trained without label smoothing and the other trained with label smoothing. The test accuracy of these GaussDerResNets on the regular STL-10 dataset was compared to three strong baseline models, the Wide Residual Network (WideResNet) by Zagoruyko and Komodakis (2016), the Harmonic Wide Residual Network (Harm-WideResNet) by Ulicny et al. (2019), and the SESN-B network by Sosnovik et al. (2020).

The results from this comparative study are presented in Table 3. As can be seen from the table, the GaussDerResNets using label smoothing during the training process achieve very good performance on the original STL-10 dataset, demonstrating near-parity with several competing methods, and showing only a 2% difference in accuracy relative to SESN-B, which is the best performing model. Notably, however, the GaussDerResNets achieve this level of classification accuracy while using five times less network parameters.

This demonstrates that the single-scale-channel GaussDerResNets are capable of handling classification on complex image datasets at a level comparable to other well performing networks, while additionally obeying

Network	#Params	Test accuracy
GaussDerResNet (no LS)	2.1M	88.05%
WideResNet	11M	88.52%
GaussDerResNet (with LS)	2.1M	89.36%
Harm-WideResNet	11M	90.45%
SESN-B	11M	91.49%

Table 3: Comparison of the test accuracies and the numbers of parameters of networks trained on the original STL-10 dataset, showing the performance obtained by (i) the single-scale-channel GaussDerResNet trained without label smoothing (abbreviated as “no LS”), (ii) the single-scale-channel GaussDerResNet trained with label smoothing, (iii) the Wide Residual (WideResNet) network (Zagoruyko and Komodakis 2016), (iv) the Harmonic Wide Residual (Harm WideResNet) network (Ulicny et al. 2019), and (v) the scale-equivariant steerable (SESN-B) network (Sosnovik et al. 2020). We can see that GaussDerResNets can achieve accuracies comparable to the other well performing networks, though marginally lower to the best performing one, while making use of far fewer network parameters.

scale covariance properties and a network design that makes it possible to extend the architecture to become scale invariant, by adding additional scale channels at different scale levels, with shared weights.

6.2 Scale generalisation experiments with multi-scale-channel GaussDerResNets on rescaled datasets

In this section, we will compare the scale generalisation abilities of the multi-scale-channel Gaussian derivative residual networks (GaussDerResNets) to the Gaussian derivative networks (GaussDerNets), where the latter were explored in our previous work in Perzanowski and Lindeberg (2025c) on the rescaled Fashion-MNIST and CIFAR-10 datasets. We will also demonstrate the scale generalisation properties of the GaussDerResNets on the new rescaled version of the STL-10 dataset.

Using multi-scale-channel networks is key to achieving good scale generalisation, as regular not scale-covariant deep networks typically fail on this task, see Appendix A.1.

Additionally, we will compare the influence of basing the networks on different permutation-invariant scale pooling methods on the scale generalisation performance. All these experiments are characterised by the fact that the networks are trained at only a single scale (object size), while the evaluation is performed on a set of copies of the test dataset, with each copy rescaled by a single size factor.

6.2.1 Scale generalisation experiments with multi-scale-channel networks on the rescaled Fashion-MNIST dataset

For the rescaled Fashion-MNIST dataset, the multi-scale-channel GaussDerResNets were trained following the training configuration outlined in Section 5, using scale channels with $\sigma_{i,0} \in \{1/(2\sqrt{2}), 1/2, 1/\sqrt{2}, 1, \sqrt{2}, 2\}$. As the objects are centred within the image frame for this dataset, we based all the networks on central pixel extraction as the spatial selection method.

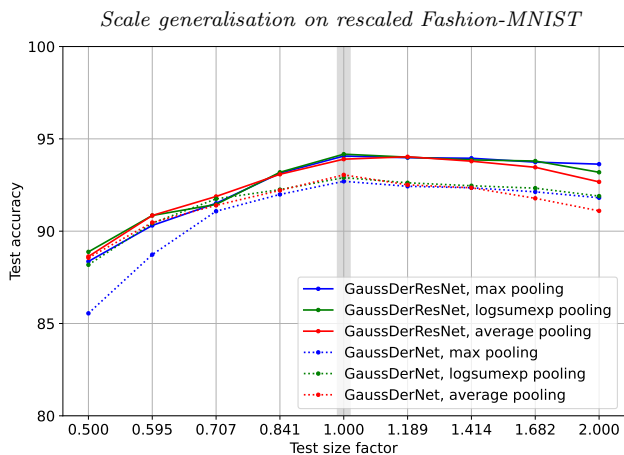


Fig. 7: Comparison between the scale generalisation curves for multi-scale-channel GaussDerResNets based on either max, logsumexp or average pooling over scale, to multi-scale-channel GaussDerNets based on max, logsumexp or average pooling over scale (reproduced from Perzanowski and Lindberg (2025c)) on the rescaled Fashion-MNIST dataset. For the test data with the same size factor 1 as the training data, represented by the shaded grey region, the GaussDerResNets achieved an accuracy of $\sim 94\%$, which is ~ 1.5 ppt higher compared to the GaussDerNets. From the graph, we can see that the GaussDerResNets have slightly better overall performance compared to the GaussDerNets, while retaining very good scale generalisation, in agreement with the theoretical analysis.

The results from this experiment are presented in Figure 7, with the networks trained on the training image data for the original size factor 1 and evaluated on the rescaled copies of the test dataset for all the possible size factors ranging from $1/2$ to 2 , and using multi-scale-channel networks based on either max, logsumexp or average pooling over scales. The results in the graph show that the performance of the GaussDerResNets is mostly flat over scales, demonstrating that the scale covariance properties derived in Section 3.1.2 hold in practice. We can also see that the GaussDerResNets achieve slightly flatter scale generalisation curves compared to the GaussDerNets for the size factors > 1 , and

becoming almost completely flat for the max pooling based network, and also outperforming the GaussDerNets by ~ 1.5 ppt. The minor drop in the performance for the GaussDerResNets, present at the smaller size factors and resulting in a similar level of performance as for the GaussDerNets at the finest scales, is likely due to discretisation effects and loss of information, caused by the fact that the original dataset consists of small objects, which are challenging to distinguish at the resulting lower effective resolution.

Concerning the behaviour of the different permutation-invariant scale pooling methods, max pooling has the best scale generalisation at the larger size factors, while average pooling and logsumexp pooling have the best scale generalisation at the smaller size factors, for both the GaussDerResNets and the GaussDerNets. Interestingly, the GaussDerResNets based on max pooling over scales generalise well for smaller size factors, which the corresponding GaussDerNets are unable to do.

For the rescaled Fashion-MNIST dataset, we leave the analysis of the scale selection properties of the GaussDerResNets to Appendix A.3, where the effect of the use of label smoothing on the scale selection properties is also investigated.

6.2.2 Scale generalisation and scale selection experiments with multi-scale-channel GaussDerResNets on the rescaled CIFAR-10 dataset

Figure 8 shows corresponding scale generalisation experiments for the rescaled CIFAR-10 dataset. As can be seen from the results, for the GaussDerResNets the test accuracy obtained on the training scale, meaning the size factor 1, shows substantial relative improvement in performance of about 7 ppt compared to the GaussDerNets. The scale generalisation curves obtained for the GaussDerResNets are significantly flatter compared to the GaussDerNets, especially the max pooling and logsumexp pooling based methods, showing up to ~ 13 ppt relative improvement in accuracy for the larger size factors, and up to ~ 8.5 ppt relative improvement in accuracy on the smaller size factors.

Furthermore, we can see that the GaussDerResNets based on max pooling or logsumexp pooling outperform the average pooling based network across all the size factors, demonstrating that the pooling methods, where a single scale channel dominates the prediction decision, achieve both the best performance on the size factor 1 and the best scale generalisation.

From the scale-covariant property of the GaussDerResNets, it would be expected that the scale-channels selected by the scale selection mechanism would increase proportionally to scaling transformations of the

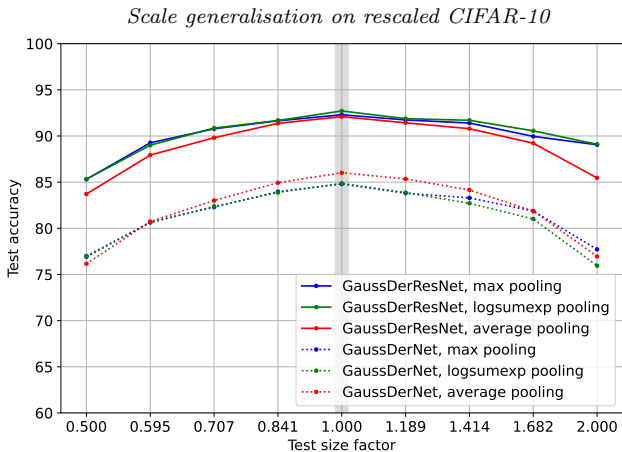


Fig. 8: Comparison between the scale generalisation curves for the multi-scale-channel GaussDerResNets based on either max, logsumexp or average pooling over scales, to multi-scale-channel GaussDerNets based on max, logsumexp or average pooling over scale (reproduced from Perzanowski and Lindberg (2025c)) on the rescaled CIFAR-10 dataset. Each network was trained on training data for size factor 1, and then evaluated on test data covering all the size factors between 1/2 and 2, with each copy of the test set only containing images at a single given scale. For the test data with the same size factor 1 as the training data, represented by the shaded grey region, the GaussDerResNets achieved an accuracy of 92.1-92.7%, which is ~ 7 ppt higher compared to the GaussDerNets. From the graph we can also clearly see that the scale generalisation properties of the GaussDerResNets are better compared to the GaussDerNets.

input data. This property can be experimentally verified by inspecting so-called scale selection histograms, constructed by accumulating information about the relative contribution of each scale channel to the classification of test samples, for each spatial scaling factor.

Figure 9 depicts the scale selection histograms for the networks based on max, logsumexp and average pooling over scales for the experiments on the rescaled CIFAR-10 dataset, trained without label smoothing. As can be seen, there is a clear and distinct linear trend for the networks based on max pooling and logsumexp pooling, a property similar to classical methods for automatic scale selection. For the network based on average pooling over scales, the trend is also linear, although less localised and more spread out. This behaviour is expected, as average pooling combines information across all the scale channels, thus enabling more scale channels to contribute to the classification.

Finally, we can note that the GaussDerResNets show roughly similar performance and parameter efficiency

on the size factor 1 of the rescaled CIFAR-10 dataset⁷, compared to other networks based on Gaussian derivative operators designed for handling image data at different scales, see for example Pintea et al. (2021) for corresponding results on the regular CIFAR-10 dataset, while having the additional property of being scale invariant, and achieving very flat scale generalisation curves.

6.2.3 Scale generalisation and scale selection experiments with multi-scale-channel networks on the rescaled STL-10 dataset

Figure 10 shows the result of corresponding scale generalisation experiments on the rescaled STL-10 dataset. Unlike the GaussDerResNet architectures used in the previous sections, these experiments use networks with layers that include a zero-order term (except in the first layer), according to Equation (50), since that choice has been found to perform significantly better on this dataset, as detailed further in Section 7.1.

Since the objects in the STL-10 dataset are not centered in the image domain, we throughout made use of spatial max pooling as the spatial selection mechanism. Label smoothing was used during the training of the max pooling and the logsumexp pooling based networks, but not for the average pooling network.

As can be seen from the results, for the GaussDerResNets based either on logsumexp or average pooling over scales, we obtain rather flat scale generalisation curves, with a drop in performance of only ~ 2 ppt between the size factors 1 and 2, thereby demonstrating very good scale generalisation capability. For the size factors 1 to 1/2, we find a clear and gradual drop in performance in the range of up to 8–11 ppt, likely due to discretisation effects and possibly also caused by the mirror extensions in the test images at the smaller size factors. The latter effect may, however, largely be an artefact of how the image dataset has been constructed and not because of the deep learning architecture.

Additionally, we can clearly see that average pooling is the best performing scale pooling method for this dataset. This differs from the GaussDerResNet behaviour on the rescaled CIFAR-10 dataset, where average pooling was outperformed by other scale pooling methods. For this dataset, logsumexp pooling performs significantly better than max pooling over most of the range, except for the largest size factors, where max pooling performs better.

In this context, it can be notable to observe that because of the scale invariant properties of the network

⁷ Training a single-scale-channel GaussDerResNet with 10M network parameters, using appropriate settings, leads to about 94.5 % accuracy on the regular CIFAR-10 dataset.

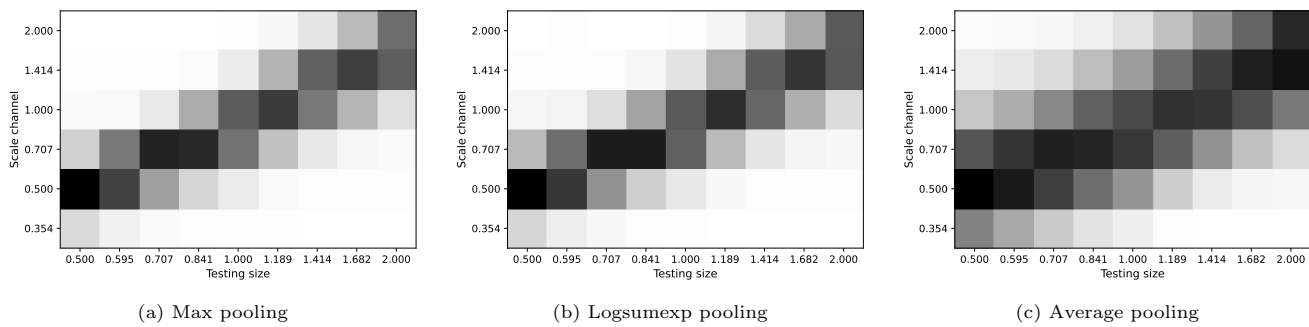


Fig. 9: Scale selection histograms for the multi-scale-channel GaussDerResNets trained and evaluated on the rescaled CIFAR-10 dataset, with no label smoothing used during training, for the three different permutation invariant aggregation methods for pooling over scales, including (a) max pooling, (b) logsumexp pooling and (c) average pooling. In these scale selection histograms, the vertical axis represents the relative contribution of each scale channel to the final classification as function of the different size factors for the test dataset as mapped onto the horizontal axis. A clear linear trend can be seen in all the three histograms, with the dominant selected scale levels, represented by the dark regions, found to be directly proportional to the size factor of the test images. This behaviour is an explicit manifestation of the scale covariant properties of the GaussDerResNet architecture.

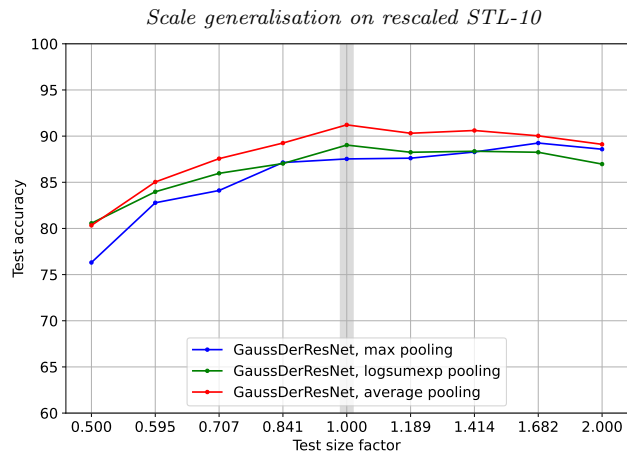


Fig. 10: Scale generalisation curves for multi-scale-channel GaussDerResNets using either max, logsumexp or average pooling over scales, with a complementary spatial max pooling spatial selection stage, on the new rescaled STL-10 dataset. In this experiment, the networks were trained on training data corresponding to size factor 1, and were then evaluated on rescaled copies of the test set covering all the size factors between 1/2 and 2, with each copy corresponding to a different single size factor. The best performing multi-scale-channel network achieved an accuracy of 91.2% on test data with the same object size (size factor 1) as the training data, represented by the shaded grey region in the graph. As can be seen in the figure, despite a portion of the STL-10 images containing non-centered objects, the multi-scale-channel GaussDerResNets based on logsumexp and average pooling lead to rather flat scale generalisation curves.

architecture, the network is not constrained to using image data of the same size (pixel count) in the testing data as used in the training data.

Figure 11 shows the scale selection histograms for the corresponding networks. On this dataset the networks show a somewhat less localised linear trend, with a shift to relatively finer scale channels being used at corresponding size factors, compared to the results for networks trained on the rescaled CIFAR-10 shown in Figure 9. This is likely due to the use of spatial max pooling as the spatial selection mechanism, which benefits from allowing different scales to be considered at different spatial locations, resulting in more neighbouring scale channels involved in the final prediction, and fine scale image structures being more impactful for computing the prediction. There is, however, a slight but noticeable flattening towards relatively coarser scale channels of the scale selection trend at small size factors, likely caused by the presence of significant mirror extension in the test images and discretisation effects.

In summary, these results demonstrate that incorporating the spatial max pooling mechanism into the GaussDerResNet architecture does preserve the desired scale covariance and scale selection properties of the network, while enabling the handling of non-centred image structures by introducing the ability to focus on any spatial location within the image, at different scales.

7 Ablation and comparative studies

This section presents ablation and comparative studies of GaussDerResNets and their variants, performed using the rescaled Fashion-MNIST, CIFAR-10 and STL-10 datasets. Here, we will examine the results of experiments dealing with different architectural variations:

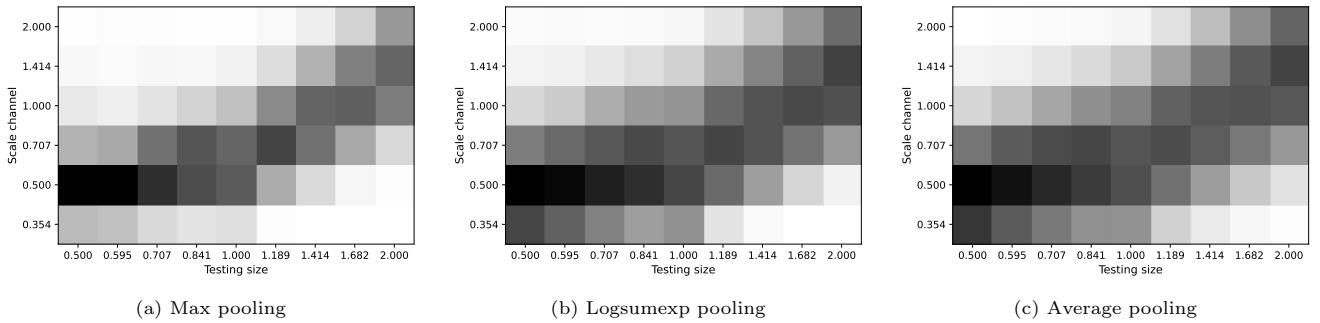


Fig. 11: Scale selection histograms for the multi-scale-channel GaussDerResNets trained and evaluated on the rescaled STL-10 dataset, for the three different permutation invariant methods for pooling over scales, including (a) max pooling, (b) logsumexp pooling and (c) average pooling. In these scale selection histograms, the vertical axis represents the relative contribution of each scale channel to the final classification as function of the different size factors for the test dataset as mapped onto the horizontal axis. Similar to the results obtained for the rescaled CIFAR-10 dataset, all the three scale pooling methods show a linear trend, where a larger size in the test images leads to the selection of proportionally coarser scale levels. This confirms that incorporating spatial max pooling into the network architecture preserves the scale covariance properties of the GaussDerResNets.

- investigating the influence of extending GaussDerResNets to include a zero-order term in the 2-jet.

In appendix sections, we additionally:

- demonstrate that comparable accuracy and scale generalisation properties can be obtained from depth-wise-separable-convolution-based DSGaussDerResNets, which substantially decrease both the number of parameters and the computational cost for inference (Appendix A.2),
- demonstrate that the use of label smoothing can significantly improve the scale generalisation properties of the networks, however, with the side effect of leading to less sharp scale selection histograms (Appendix A.3),
- demonstrate that pre-training, using a first phase of single-scale-channel mode followed by a second phase of genuine multi-scale-channel training, can substantially decrease the computational work for training, and often leading to better convergence properties, compared to training a multi-scale-channel GaussDerResNet from scratch (Appendix A.4), and
- demonstrate that weight transfer to a denser scale-channel spacing can slightly improve the scale generalisation properties (Appendix A.5).

7.1 Benefit of using a zero-order term in higher layers of the networks

The receptive fields in CNNs can be related to the concept of scale-space, by approximating the filters using a Gaussian N -Jet, which is accomplished by using a basis of Gaussian derivative operators, up to a certain order N , to form a truncated local Taylor expansion,

that represents the local image structure. This kind of approximation involves a Gaussian operator of order zero, which differs from the standard layer design of the GaussDerResNet architecture, that is purposely based only on first- and second-order (scale-normalised) Gaussian derivative operators.

In this section, we will investigate how including a zero-order term in the computational primitives for the layers of GaussDerResNets (except for in the first layer), according to Equation (50), affects the scale generalisation and the scale selection properties of the network. For this purpose, for the rescaled Fashion-MNIST, CIFAR-10 and STL-10 datasets, we will perform comparative studies of the effect of using a standard vs. a zero-order based GaussDerResNet design.

For each dataset, we trained two multi-scale-channel GaussDerResNets, one with the layers defined using the standard design, according to Equation (6), and the other defined using the Gaussian N -jet with a zero-order term, according to Equation (50). The models used max pooling over scales, with the exception of average pooling being used for the rescaled STL-10 dataset network, and the training was done using the protocol and the settings described in Section 5, for each dataset.

The upper row in Figure 12 shows the resulting scale generalisation curves. For the rescaled Fashion-MNIST dataset, we can see that omitting the zero-order terms results in slightly better performance, as well as improved scale generalisation for the smaller test size factors. For the rescaled CIFAR-10 dataset, we can see that the performance at the size factor 1 is better when basing the network on layers with the zero-order terms included. The scale generalisation curve is, however, sig-

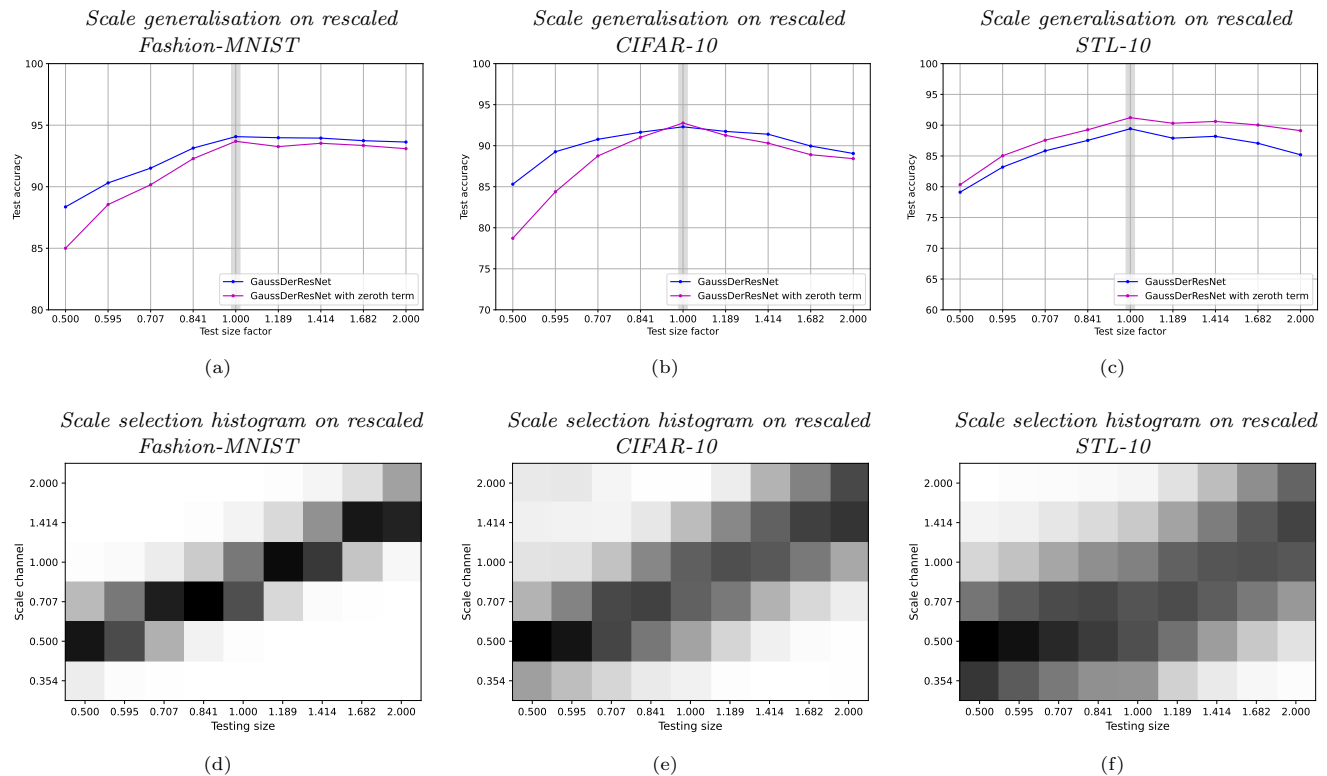


Fig. 12: Comparison between the scale generalisation curves and the corresponding scale selection histograms for the multi-scale-channel GaussDerResNets, based on either standard 2-jet layers or 2-jet layers complemented with a zero-order term, on the rescaled (left) Fashion-MNIST, (middle) CIFAR-10 and (right) STL-10 datasets. The left and middle subfigures use networks based on max pooling over scales, while the rightmost subfigure uses networks based on average pooling. After being trained on the training set for the size factor 1, the networks were tested on all the size factors between 1/2 and 2. The scale selection histograms visualise the relative contribution of each scale channel to the final classification. As can be seen from the graphs, including a zeroth-order term clearly improves both the accuracy and the scale generalisation for the rescaled STL-10 dataset. For the rescaled Fashion-MNIST and CIFAR-10 datasets, using a zeroth-order term does not lead to any improvement, with the performance at the smaller size factors noticeably reduced when including this term. Additionally, a clear linear trend can be seen in the scale selection histograms for all the three datasets, demonstrating that including a zero-order term in the computational primitives of the GaussDerResNets leads to the selected scale levels still being proportional to the size in the test image data, as expected from theory. (Note that the vertical axes for the test accuracy in the top subfigures use different lower bounds for the different datasets.)

nificantly less flat at the smaller size factors compared to the standard GaussDerResNet.

The results for the rescaled STL-10 dataset show a notably different behaviour, where both the test accuracy and the scale generalisation is significantly better when including zero-order terms. When basing the layers on zero-order terms, the performance for the size factor 1 improves by ~ 2 ppt, and the performance at the large size factors is also clearly improved, with the performance at the size factor 2 improving by ~ 4 ppt.

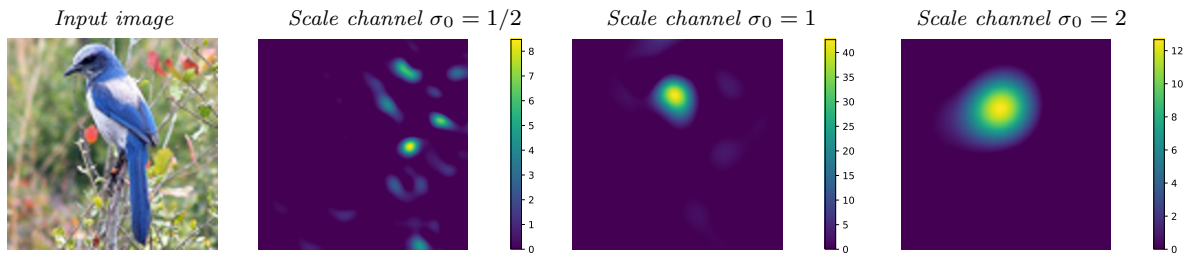
The corresponding scale selection histograms are shown in the bottom row in Figure 12. A clear linear trend between the selected scale levels and the size of the images can be observed for each rescaled dataset, indicating that including the zero-order terms in the layers of the GaussDerResNets results in scale covari-

ance properties consistent with the theoretical analysis in Section 3.1.

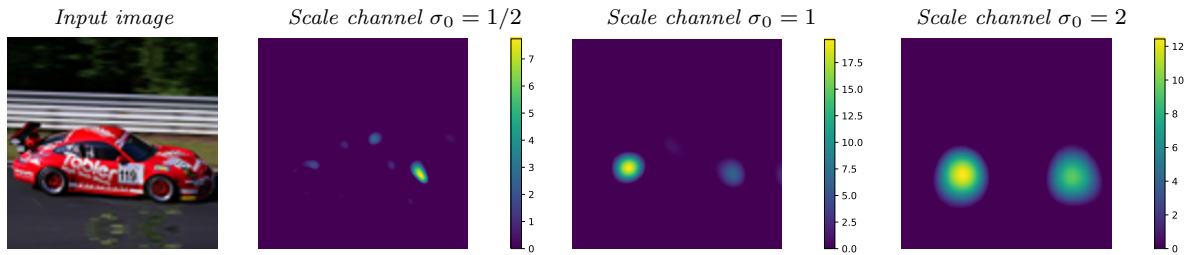
8 Visualisations of Gaussian derivative ResNets

To facilitate a deeper understanding of the multi-scale-channel GaussDerResNets in operation, we will in this section analyse visualisations of the activation maps in the final convolution layer before the spatial selection stage, for the rescaled STL-10 dataset.

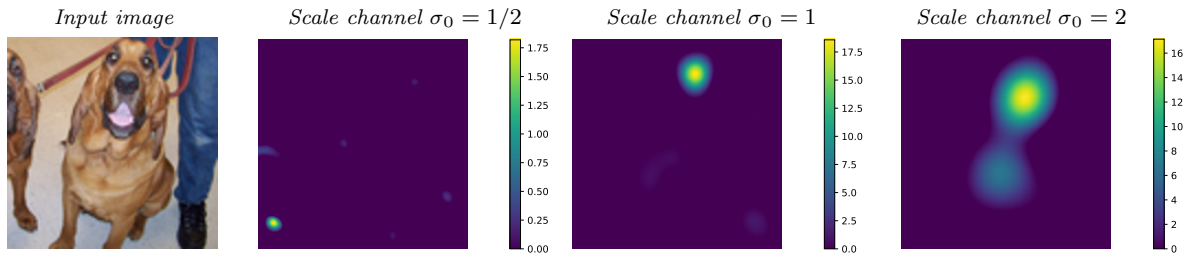
In Appendix A.6, we also analyse the effective filters learned by the GaussDerResNets with the layers based on zero-order terms.



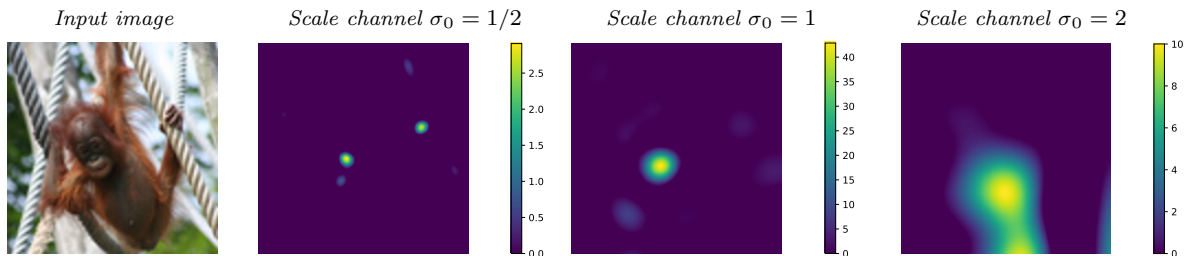
(a) Activation maps from different scale channels for a sample image from the class “bird”.



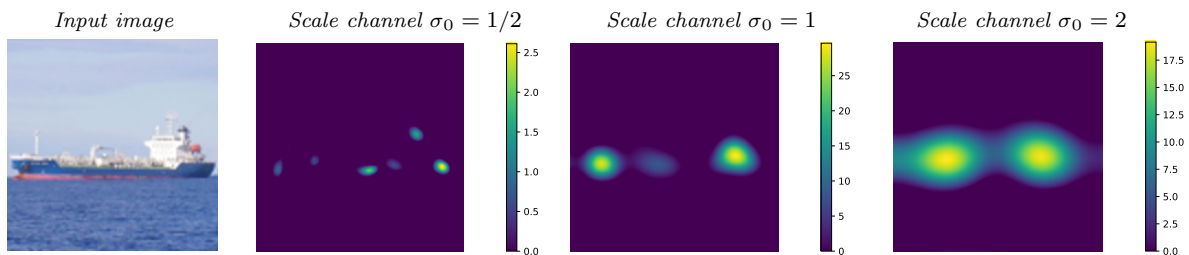
(b) Activation maps from different scale channels for a sample image from the class “car”.



(c) Activation maps from different scale channels for a sample image from the class “dog”.



(d) Activation maps from different scale channels for a sample image from the class “monkey”.



(e) Activation maps from different scale channels for a sample image from the class “ship”.

Fig. 13: Activation maps of correctly classified images from the rescaled STL-10 dataset, extracted from the final layer of a multi-scale-channel GaussDerResNet with a spatial selection stage based on spatial max pooling and scale selection stage based on average pooling over scales. The activation maps reveal which spatial areas within the image elicit strong responses at the feature channel corresponding to the correct class, for scale channels based on initial scale values $\sigma_0 \in \{1/2, 1, 2\}$, given test samples chosen from size factor 2 test set. Each row depicts results from one of the five chosen classes: (a) “bird”, (b) “car”, (c) “dog”, (d) “monkey” and (e) “ship”. As can be seen from the subfigures, the network typically makes a prediction by identifying characteristic parts of objects, either at fine or coarse scales, which correspond to strong responses at finer scale channels or coarser scale channels, respectively.

8.1 Activation maps of networks with zero-order terms

In this section, we will inspect the feature maps in the final convolution layer, often referred to as activation maps, for the GaussDerResNets with the computational primitives of the layers extended to include zero-order terms and trained on the rescaled STL-10 dataset using spatial max pooling as the spatial selection mechanism. As previously mentioned, this enables the network to focus on objects at any location in the image domain.

Notably the layers in the GaussDerResNets are directly interpretable due to the absence of spatial subsampling operations, such as strided convolutions, thus enabling a direct mapping between the image structures and their corresponding activations at different scales.

Five illustrative correctly classified images were selected from the classes “bird”, “car”, “dog”, “monkey” and “ship”, and chosen from the test set for the size factor 2, where there is no mirroring in the image data. The activations were computed at fine, medium or coarse scales, achieved by extracting the output of the final layers of the scale channels $\sigma_0 = \{1/2, 1, 2\}$, respectively, for the feature channel corresponding to the ground-truth class of the input image.

Figure 13 depicts the generated activation maps, along with colour bars for the strength of the response. We can see that, due to the use of spatial max pooling as the spatial selection method, the network is capable of localising characteristic image structures and features at any spatial position within the image, even close to the boundary. The finer scale channels typically focus on fine scale textures and body/machine parts, such as paws, mouths or car parts. The coarser scale channels focus on coarse scale image structures, such as heads, torsos or larger machine parts. In fact, we see that the network is capable of detecting multiple maxima corresponding to image structures key for making a prediction, despite the fact that only a single global maximum is selected during the classification stage. Additionally, the sizes of the activation regions are seen to be proportionally larger for larger scale channels, as expected from the scale-covariant properties of the network.

The depicted activation maps have quite intuitive explanations. For the bird, the medium scale channel focuses on the head, while the fine scale focuses on the background, which may help classification. For the car, there is a main focus on the wheels. For the dog, the main focus is on the head and the torso. However, the finer scale channel focuses on the other paw of the nearby dog. For the monkey, the main focus is on the mouth. The coarser scale focuses on the torso, whereas the fine scales focus on smaller body parts. For the boat, the medium and the coarser scale channels focus on the

bow and the stern of the boat. The finer scale channels focus on smaller parts of the boat.

In this way, these results illustrate how the spatial selection scheme, in combination with the pooling method over scale, is able to automatically learn and classify characteristic structures for the objects in the respective classes in the dataset.

9 Summary and conclusions

We have proposed the notion of scale-invariant Gaussian derivative residual networks (GaussDerResNets) and presented an extensive investigation of their performance and scale generalisation properties, including architectural variants based on structural modifications. Additionally, we have examined the effectiveness of new training approaches on rescaled image datasets, where the corresponding test sets contain spatial scaling variations not encountered during training. The ability to handle different scales in image data is built in as prior knowledge into the GaussDerResNet architecture, thereby enabling the networks to generalise to scales not seen during training—a property which most other deep network architectures do not include in their design. This is achieved by ensuring scale covariance of the receptive fields based on linear combinations of scale-normalised Gaussian derivatives coupled in cascade, with weight sharing between the scale channels and permutation invariant pooling over scales.

Building upon earlier work in Lindeberg (2022) and Perzanowski and Lindeberg (2025c), where Gaussian derivative networks (GaussDerNets) without residual connections were proposed and investigated experimentally, the GaussDerResNets proposed in this paper substantially modernise and improve this architecture in several respects, such as the incorporation of scale covariant residual blocks and considerably increased network size and depth, which in this work is demonstrated to lead to significantly better performance and scale generalisation properties on natural image datasets.

For the GaussDerResNet architecture, we have described its theoretical properties in Section 3, with formal proofs of scale covariance and scale invariance properties, as well as structural relations to semi-discretisations of the diffusion equation. We have also described extensions to depthwise-separable convolutions and zero-order terms, which we then have investigated experimentally by ablation studies in Appendix A.2 and in Section 7.1.

To investigate how scaling variations affect the performance of GaussDerResNets, we have in Section 4.1.3 defined a new rescaled STL-10 dataset, which incorporates systematic spatial scaling variations. Compared

to the previously existing rescaled MNIST, Fashion-MNIST and CIFAR-10 datasets, this dataset is more challenging, has higher image resolution and contains far less training data.

In experimental investigations of the classification performance and the scale generalisation properties of the new GaussDerResNet architecture, we have in Section 6 demonstrated that this network architecture achieves noticeably better performance on the rescaled Fashion-MNIST dataset, and significantly better performance on the rescaled CIFAR-10 dataset, compared to the previously proposed GaussDerNets without residual connections. We have also demonstrated that the here proposed GaussDerResNet architecture allows for good classification performance on the regular STL-10 dataset without scaling variations as well as good scale generalisation properties on the new rescaled STL-10 dataset with spatial scaling variations.

In these experiments, we notably found that not including a zero-order term was preferable for the rescaled Fashion-MNIST and CIFAR-10 datasets, while including a zero-order term was strongly beneficial for the rescaled STL-10 dataset. For the STL-10 dataset, we also included a spatial selection mechanism based on spatial max pooling to handle non-centred objects in the image domain. From our in-depth analysis of the scale selection properties of the networks, we specifically found that the selected scale levels increased linearly with the spatial scaling factors in the underlying test data, in agreement with the expected theoretical behaviour, for all the studied types of scale pooling mechanisms in terms of max pooling, logsumexp pooling, or average pooling.

To gain a better understanding of the properties and behaviour of the GaussDerResNets under different settings and conditions, we have in the appendix sections performed a set of additional ablation studies. These comprise exploring a new architectural variant of GaussDerResNets, where we studied modernisations of the architecture to include depthwise-separable convolutions, which significantly reduces the number of model parameters. Specifically, we demonstrated that this architecture retains provably scale covariant and scale invariant properties and can maintain good performance and scale generalisation properties. The depthwise-separable networks are, however, harder to train.

Furthermore, in the Appendix, we investigated the effectiveness of new training methods for GaussDerResNets, where we:

- demonstrated that pre-training a multi-scale-channel network by initialising its weights with the weights from a trained single-scale-channel network reduces the amount computation required to achieve good

optimisation during its training, and often improving the scale generalisation at fine scales, and

- found that increasing the number of scale channels in a multi-scale-channel GaussDerResNet through weight transfer after training results in a slight improvement of its scale generalisation properties.

Finally, in Section 8, we examined the activation maps, demonstrating that the GaussDerResNets have good explainability properties in terms of the regions of interest, producing strong responses at characteristic image structures that identify the objects in the images.

To conclude, the purpose of this paper has been to show that the scale-invariant GaussDerResNet architecture, including its variants as presented here, can be trained in a stable and successful manner, and can achieve very good classification performance and scale generalisation on natural image datasets with spatial scaling variations, thereby being able to handle test data that contain objects at scales not present in the training data. We argue that such scale generalisation constitutes an important property for deep networks aimed at image classification under large scaling variations. Specifically, provably scale-covariant and scale-invariant deep network architectures, which enforce scaling symmetries, allow for a theoretically well-defined, consistent and interpretable treatment of the scaling variations commonly encountered in real-world data, thereby reducing reliance on data augmentation and/or larger amounts of training data.

Acknowledgements

The computations were enabled by resources provided by the National Academic Infrastructure for Supercomputing in Sweden (NAISS), partially funded by the Swedish Research Council through grant agreement no. 2022-06725, as well as on other GPU resources provided by the PDC Center for High Performance Computing at KTH Royal Institute of Technology in Sweden.

A Appendix

This appendix addresses the following topics:

- Appendix A.1 shows the *scale generalisation properties of single-scale-channel networks* applied to the rescaled Fashion-MNIST, CIFAR-10 and STL-10 datasets, demonstrating that the accuracy of the networks may decrease substantially with increasing differences between the scales in the training data vs. the testing data.

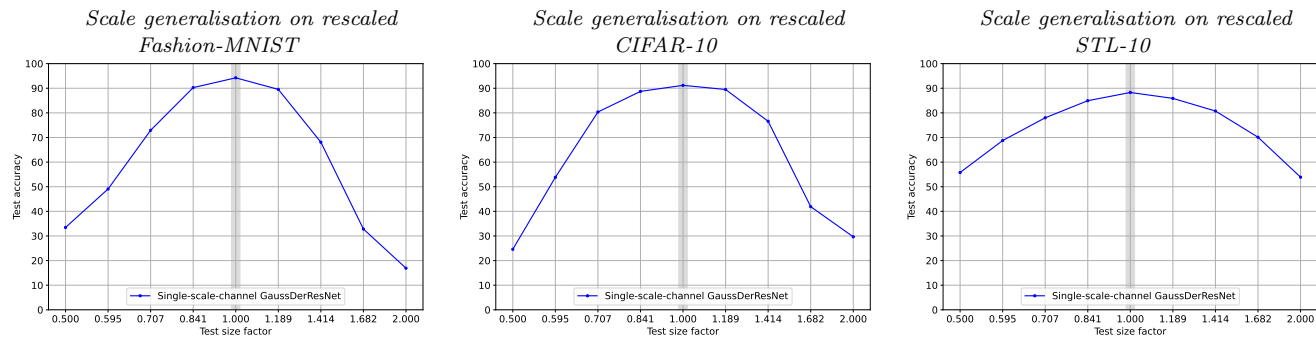


Fig. 14: Scale generalisation curves for the single-scale-channel GaussDerResNets on the rescaled (left) Fashion-MNIST, (middle) CIFAR-10 and (right) STL-10 datasets. Test data with the same size factor 1 as the training data is represented by the shaded grey region. Note that the vertical axes for the test accuracy are in the range 0–100%, unlike the scale generalisation graphs in the main paper.

- Appendix A.2 explores the *extension of GaussDerResNets to depthwise-separable-convolution-based DS-GaussDerResNets*, thereby reducing both the number of parameters in the network and the computational cost, by reusing the spatial components of the convolutions, with reasonably maintained accuracy and scale generalisation properties.
- Appendix A.3 shows the *influence of label smoothing on the scale generalisation and the scale selection properties*, demonstrating that label smoothing leads to better scale generalisation properties, while also leading to less sharp scale selection histograms.
- Appendix A.4 introduces a notion of *pre-training*, where in a first phase a single-scale-channel network is trained on the training data, after which in a second phase the weights are transferred to training a multi-scale-channel network to achieve genuine multi-scale-channel training. In this way, *the training cost is substantially reduced, while at the same time often leading to better convergence properties* compared to training a multi-scale-channel network from scratch.
- Appendix A.5 explores a *mechanism of weight transfer, to achieve a denser spacing of the scale channels in the testing phase* than in the training phase, and demonstrates that this can lead to slight increases in the accuracy and the scale generalisation properties. In this way, we significantly reduce the amount of computation during training compared to training a dense network from scratch, while leading to a proportional increase in the amount of computations during inference.
- Appendix A.6 shows *visualisations of the learned effective filters* in different layers of the Gaussian derivative ResNets based on zero-order terms applied to the rescaled STL-10 dataset, thereby visu-

alising the types of receptive fields that the Gaussian derivative ResNet architecture is based on.

A.1 Scale generalisation properties of single-scale-channel networks

Regular deep networks without in-built scale covariance or scale invariance properties will typically have very poor scale generalisation properties. We demonstrate this by training single-scale-channel GaussDerResNets, which lack the scale invariance property of their multi-scale-channel counterparts, on the rescaled Fashion-MNIST, CIFAR-10 and STL-10 datasets. These single-scale-channel networks were trained in the same manner as the multi-scale-channel networks according to Sections 5 and 6 in the main body of the paper (although using larger batch sizes of 64 for the rescaled Fashion-MNIST and STL-10 datasets and 128 for the rescaled CIFAR-10 dataset), with each network based on the initial scale level $\sigma_0 = 1$.

Figure 14 shows the results from this experiment, where the training is performed for the single size factor 1, and testing is performed for all possible size factors between 1/2 and 2. From the graphs, we can see that for all the datasets the testing accuracy drops sharply for size factors other than 1, with the loss in performance becoming larger, the further away the testing scale is from the training scale. Additionally, from the results for the rescaled STL-10 dataset we see that the scale generalisation curve is somewhat flatter than for the other datasets, which may be due to the presence of different scales within the original dataset used for training, thus serving as a type of data augmentation.

	rescaled Fashion-MNIST	rescaled CIFAR-10	rescaled STL-10
# network parameters (GaussDerResNets)	295k	1.78M	2.07M
# network parameters (DSGaussDerResNets)	120k	547k	669k

Table 4: Number of network parameters for the multi-scale-channel GaussDerResNets and DSGaussDerResNets employed in our experiments, for the three rescaled datasets.

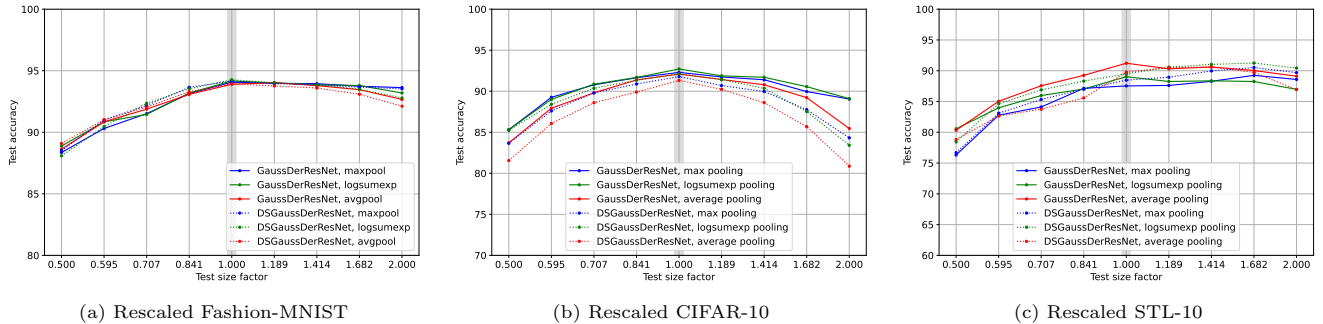


Fig. 15: Comparison between the scale generalisation curves for the multi-scale-channel GaussDerResNets and the depthwise-separable GaussDerResNets (DSGaussDerResNets), with the networks based on scale selection using either max, logsumexp or average pooling over scales, and trained on the rescaled (a) Fashion-MNIST, (b) CIFAR-10 and (c) STL-10 datasets. The training of the models was performed on the training data for the size factor 1, while the evaluation was performed on the corresponding test datasets for all the size factors between 1/2 and 2. As can be seen from the graphs, for the rescaled Fashion-MNIST and STL-10 datasets, the performance for the DSGaussDerResNets is similar to the performance of the GaussDerResNets. For the rescaled CIFAR-10 dataset, however, the performance for larger size factors is lower, probably caused by a less suitable choice of training parameters. (Note that the vertical axes for the test accuracy use different lower bounds for the different datasets.)

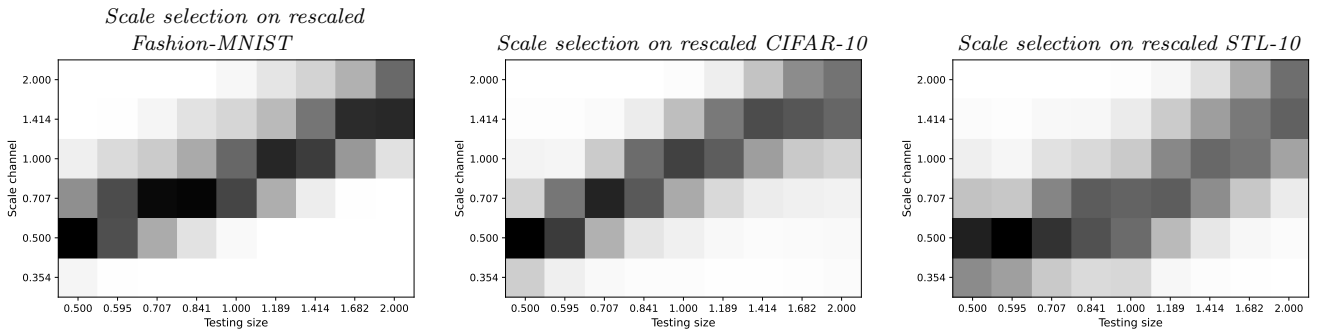


Fig. 16: Scale selection histograms for the multi-scale-channel DSGaussDerResNets based on max pooling over scales applied to the rescaled (a) Fashion-MNIST, (b) CIFAR-10 and (c) STL-10 datasets. These histograms visualise the relative contribution of each scale channel to the final classification. From these results we can see that, as expected from the theory, the GaussDerResNets based on depthwise-separable convolution operations have very similar scale selection properties as standard GaussDerResNets, with a rather clear linear trend obtained on all the rescaled datasets. This trend demonstrates that the same scale covariance properties hold between the scale channels based on standard or depthwise-separable convolutions, with the selected scale levels being proportional to the size of image features in the testing data.

A.2 Gaussian derivative networks based on standard vs. depthwise-separable convolutions

The GaussDerResNet architecture studied so far is based on standard convolutions, however, it is also possible to construct scale invariant GaussDerResNets based on depthwise-separable convolutions, referred to as DS-GaussDerResNets, as outlined in Section 3.8.2 in the main body of the paper.

Incorporating depthwise-separable convolutions into the architecture can be beneficial, as such operations may achieve comparable performance to standard convolutions, while requiring significantly fewer parameters as well as reducing the computational cost by reusing the results from the spatial convolutions. Therefore, depthwise-separable convolutions are often included in modern architectures for CNNs.

To investigate how depthwise-separable convolutions affect the performance and scale invariance properties of GaussDerResNets, we compared the test accuracy and scale generalisation of DSGaussDerResNets and GaussDerResNets on the rescaled Fashion-MNIST, CIFAR-10 and STL-10 datasets.

The DSGaussDerResNet architecture is optimised for efficiency, by basing the first and last layer, as well as the first 4 residual blocks, on standard convolutions (meaning that no fusion with a pointwise convolution stage is used), while the remaining 5 blocks are based on depthwise-separable convolutions. This design shares some similarity with the EfficientNetV2 architecture (Tan and Le 2021). Specifically, it increases the efficiency, because while depthwise convolutions are beneficial to include in the higher layers, they are computationally slow in the early layers. Due to the use of depthwise-separable convolution based layers, the DSGaussDerResNets use several times fewer network parameters than the standard GaussDerResNets. The number of network parameters for the corresponding rescaled datasets used in our experiments is shown in Table 4.

In the same manner as for the GaussDerResNets used in the experiments in Section 6 in the main body of the paper, the DSGaussDerResNets in this study used, for the most part, the parameter values and the training configurations summarised in Section 5 in the main body of the paper, with the only difference being that for the rescaled CIFAR-10 dataset we used $r = 1.22$ and for the rescaled STL-10 dataset we used an initial learning rate of 0.005 and 170 training epochs, as this was found to improve the training stability. The multi-scale-channel networks were constructed using scale channels with $\sigma_{i,0} \in \{1/(2\sqrt{2}), 1/2, 1/\sqrt{2}, 1, \sqrt{2}, 2\}$, and the training process included label smoothing and learning rate warm-up. For the rescaled Fashion-MNIST and CIFAR-10 datasets, central pixel extraction was used as the spatial selection method, while spatial max pooling was used for the rescaled STL-10 dataset. Additionally, for the rescaled STL-10 dataset, the networks were once again based on layers that include a zero-order term.

Graphs showing the resulting scale generalisation curves obtained from these experiments are shown in Figure 15. For the rescaled Fashion-MNIST dataset, which is a relatively simple dataset, we can see that there are no significant differences between the scale generalisation performance for the GaussDerResNets and the DSGaussDerResNets, with only a minor relative drop in performance found at large size factors, for the DSGaussDerResNets, and a minor relative performance increase found at small size factors.

For the rescaled CIFAR-10 dataset, we can see that the GaussDerResNets achieve higher performance on

the size factor 1, of less than 1%, compared to the DSGaussDerResNets. The scale generalisation of the GaussDerResNets is flatter compared to the DSGaussDerResNets, with the networks based on logsumexp and max pooling showing the best performance. A notable drop in performance at large size factors is observed for the DSGaussDerResNets compared to the GaussDerResNets, up to ~ 6 ppt, and only a minor drop for the smaller size factors, ranging between 0 and ~ 2 ppt. This level of performance is good, considering that the DSGaussDerResNets use almost 4 times fewer network parameters compared to the GaussDerResNets.

Additionally, for the rescaled STL-10 dataset the performance and the scale generalisation of the average pooling based GaussDerResNet is for the most part better than the DSGaussDerResNets, with between 1.5 to 3 ppt improved performance at the size factor 1. We also see that for the larger size factors, the performance curve of the DSGaussDerResNets based on max and logsumexp pooling is slightly better relative to all the GaussDerResNets, and furthermore it outperforms the GaussDerResNets based on corresponding pooling methods across all size factors, by up to 2–4 ppt.

The property that the DSGaussDerResNets attain comparable performance and scale generalisation on the rescaled CIFAR-10 and STL-10 datasets, with roughly a quarter the number of parameters, underscores the efficiency of their representations, and benefits of longer training.

Figure 16 shows the scale selection histograms for the DSGaussDerResNets trained on the rescaled Fashion-MNIST, CIFAR-10 and STL-10 datasets. The histograms were obtained by accumulating the relative contributions of each scale channel to the predictions. For each dataset, we can see a clear linear trend, similar to the behaviour of classical methods for scale selection. The good scale generalisation properties and the linear trend showcased in the scale selection histograms obtained in the experimental results in this section empirically confirm that the scale invariant properties of the GaussDerResNets also hold for the DSGaussDerResNets, in agreement with the theoretical analysis.

A.3 Influence of label smoothing on scale generalisation and scale selection

To investigate how the use of label smoothing as a regularisation technique during training may affect the scale generalisation and scale selection properties of multi-scale-channel GaussDerResNets, we performed comparative studies on networks trained with and without label smoothing, on the rescaled Fashion-MNIST, CIFAR-10 and STL-10 datasets.

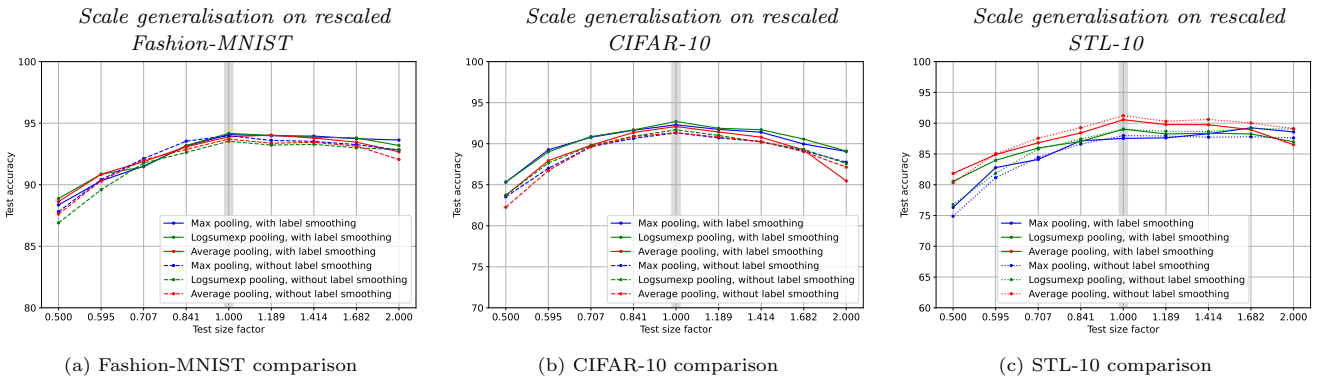


Fig. 17: Scale generalisation curves for the multi-scale-channel networks based on max, logsumexp or average pooling over scales, trained with or without label smoothing during training, for the (left) the rescaled Fashion-MNIST dataset, (middle) the rescaled CIFAR-10 dataset, and (right) the rescaled STL-10 dataset. The networks were then tested on all the size factors between $1/2$ and 2 , after training on the single size factor 1 . The graphs show that using label smoothing as an additional regularisation method during training typically results in better overall performance, while retaining good scale generalisation properties. Note that the vertical axes for the test accuracy use different lower bounds for the different datasets.

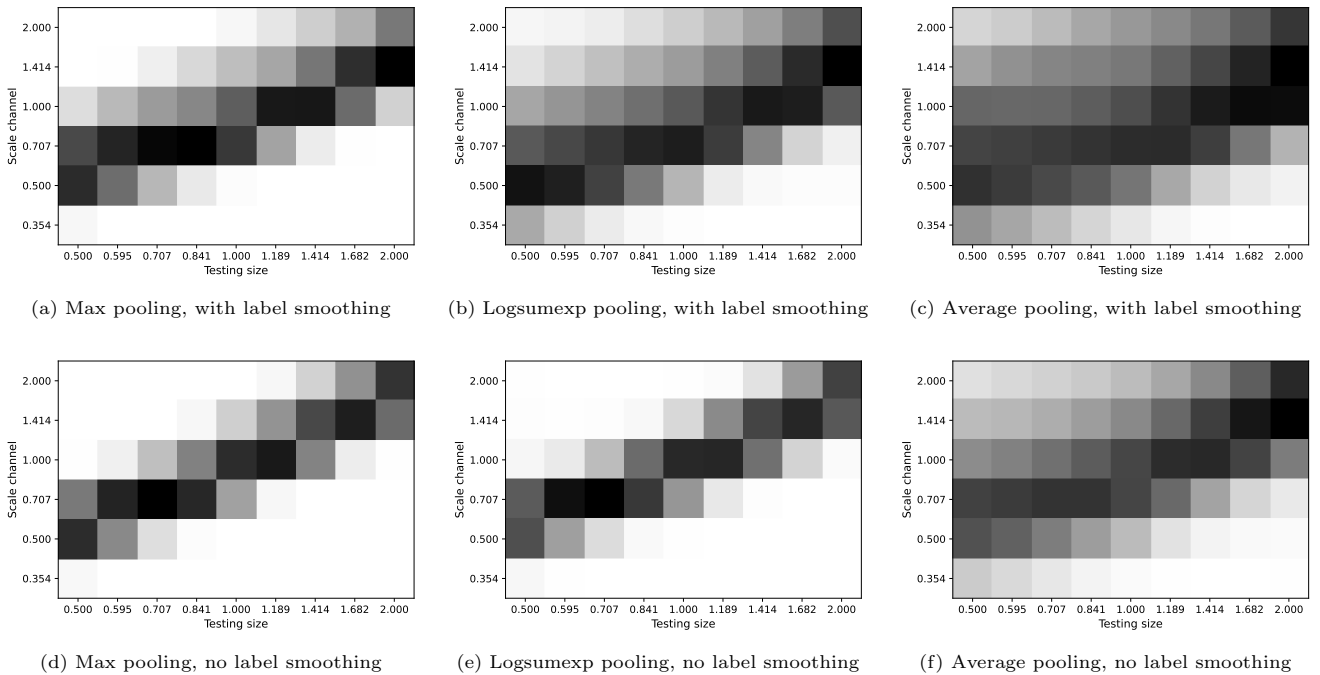


Fig. 18: Scale selection histograms for the multi-scale-channel GaussDerResNets applied to the rescaled Fashion-MNIST dataset, trained (a-c) with label smoothing and trained (d-f) without label smoothing, for all the three permutation-invariant pooling over scale methods: max, logsumexp and average pooling. The scale selection histograms demonstrate a clear linear trend between the selected scale levels (the scale channels) and the size in the testing data. We can also see that the networks based on label smoothing create more spread out and less diagonal linear trends in the scale selection histograms.

For each rescaled dataset, we trained a network for each possible permutation-invariant scale pooling approach: max pooling, logsumexp pooling or average pooling, respectively. The training was performed using the architectural parameters and training protocol described in Section 5 in the main body of the paper, using scale channels based on initial scale values $\sigma_{i,0} \in \{1/(2\sqrt{2}), 1/2,$

$1/\sqrt{2}, 1, \sqrt{2}, 2\}$. The only exceptions were the networks trained on the rescaled Fashion-MNIST dataset without the use of label smoothing, as they use slightly different training parameters, namely a weight decay value of 0.05 and scale channel dropout with $q = 0.1$.

Figure 17 shows the resulting scale generalisation curves for each rescaled dataset, for networks trained

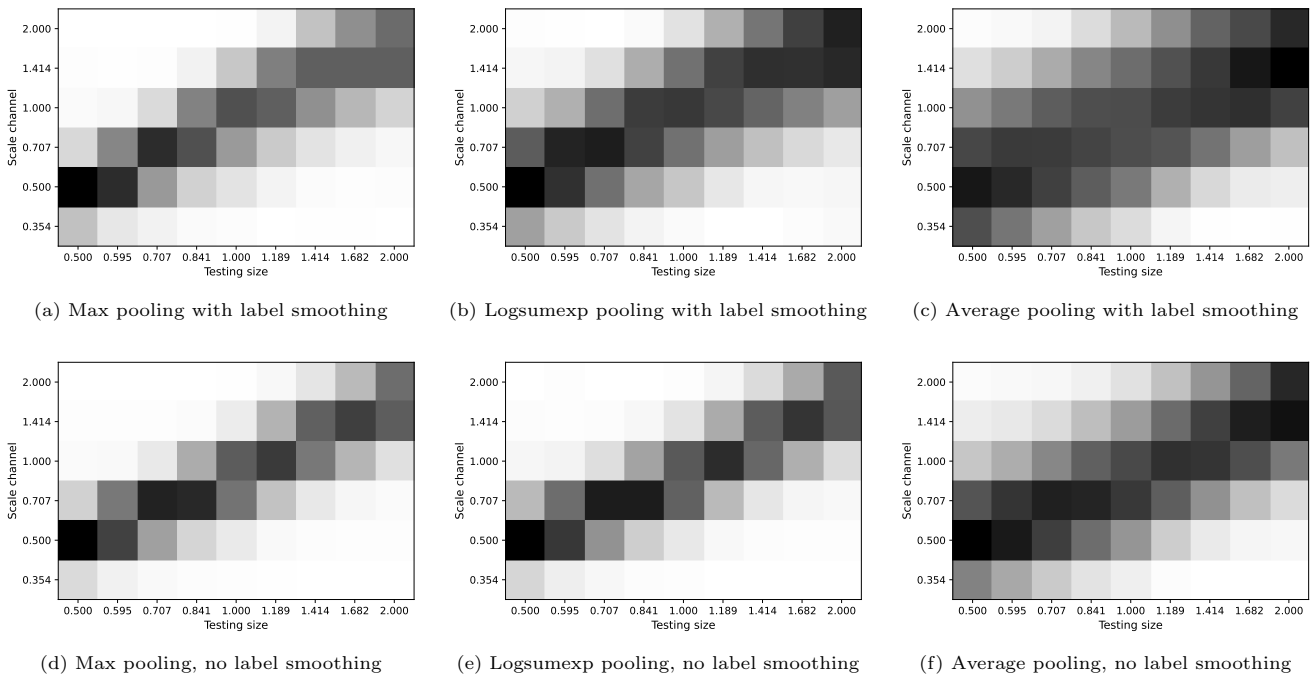


Fig. 19: Scale selection histograms for the multi-scale-channel GaussDerResNets applied to the rescaled CIFAR-10 dataset, trained (a-c) with label smoothing and trained (d-f) without label smoothing, for all the three permutation invariant pooling over scale methods: max, smooth max (logsumexp) and average pooling. The scale selection histograms demonstrate a clear linear trend between the selected scale levels (the scale channels) and the size in the testing data. Once again we can see that the networks based on label smoothing create more spread out and less diagonal linear trends in the scale selection histograms.

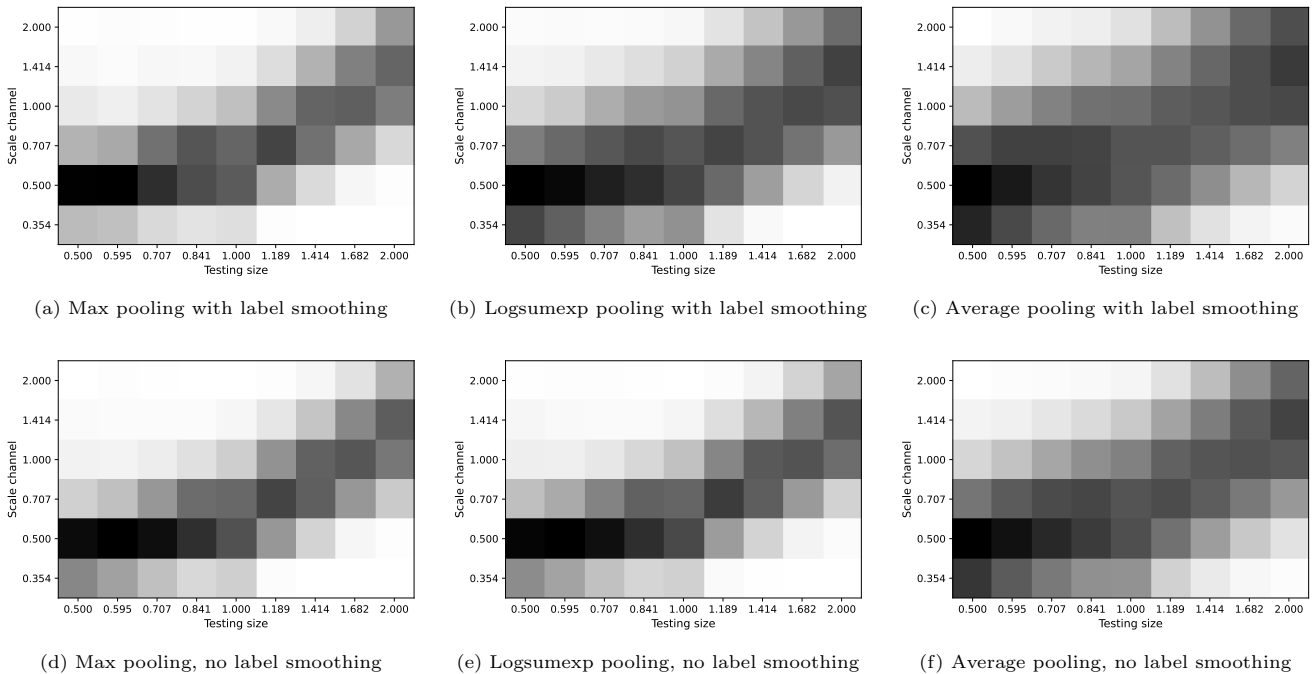


Fig. 20: Scale selection histograms for the multi-scale-channel GaussDerResNets applied to the rescaled STL-10 dataset, trained (a-c) with label smoothing and trained (d-f) without label smoothing, for all the three permutation invariant pooling over scale methods: max, smooth max (logsumexp) and average pooling. A fairly linear trend can be seen between the selected scale levels (the scale channels) and the size in the testing data, with only minor flattening at small size factors. Furthermore, we can also see that the networks trained with label smoothing have a slightly more spread out diagonal linear trends in the scale selection histograms.

on size factor 1 training data and evaluated on copies of the test set, with each copy rescaled to a single distinct spatial scale, ranging from 1/2 to 2. As we can see, using label smoothing during training results in, for the most part, better scale generalisation performance for the networks based on max or logsumexp pooling. For the networks based on average pooling, we see that on the rescaled Fashion-MNIST and CIFAR-10 dataset using label smoothing is beneficial, showing improvement in improvement at every size factor, with the only exception being size factor 2 performance for CIFAR-10. For the rescaled STL-10 dataset, however, we see that not using label smoothing leads to improved performance, with only the performance for the single size factor 1/2 showing a minor drop. For both the rescaled CIFAR-10 and rescaled STL-10 datasets, there is, however, a certain drop in performance for the largest size factors, possibly caused by the training not having sufficiently converged.

Regarding the effect that label smoothing has on the scale selection properties, Figures 18, 19 and 20 depict the corresponding scale selection histograms, which visualise the contributions from each scale channel to the final classification. We can clearly see that in each case, a linear trend is present, meaning that the size of the automatically selected scale channel is directly proportional to the size of the image structure. For the rescaled STL-10 dataset, we see that for both of the regularisation methods, the scale selection trend is shifted slightly downwards, as the use of spatial max pooling as a spatial selection methods leads to the network preferring to focus on smaller features.

We can also see that using label smoothing during training leads to a trade-off, in that the networks based on label smoothing create slightly more spread out scale selection trends, while the scale generalisation performance is generally slightly better, as already seen in Figure 17. This is not surprising, as the role of label smoothing is to prevent overconfidence in predictions, meaning that a reduction in the certainty of the prediction also leads to a minor reduction in certainty about which scale channel is the most appropriate to select.

A.4 Effects of pre-training with a single-scale-channel network on scale generalisation

The computational cost of training multi-scale-channel networks increases with the number of scale channels. Therefore, one could ask if it is possible to achieve similar or improved level of scale generalisation, while also requiring less training resources. In Barisin et al. (2024b) and Perzanowski and Lindeberg (2025c), it was

demonstrated that transferring the weights of a single-scale-channel network trained on training data with a fixed object size, to a multi-scale-channel network, greatly reduces the computational cost needed to train the network. Such an approach may, however, not reach the same level of scale generalisation performance as genuine multi-scale-channel training.

In this ablation study, we propose a modified version of this computationally efficient approach, where the training is divided into two stages: first pre-training with a single-scale-channel network,⁸ followed by post-training with a multi-scale-channel network initialised with the weights transferred from the pre-trained single-scale-channel network. This approach shares similarities with scale-space methodology, as it starts at a single scale and then evolves into a multi-scale optimisation problem, thereby sharing similarities with Gaussian scale-space generation through smoothing or the linear diffusion paradigm, see Lindeberg (1993).

We explore the viability of this approach on the rescaled Fashion-MNIST, CIFAR-10 and STL-10 datasets, by comparing the scale generalisation performance of networks trained with this method to networks fully trained using genuine multi-scale-channel training from Section 6.2 in the main body of the paper.

For these pre-training experiments, we used two training stages instead of one, each using different values of the batch size, the initial learning rate and the number of epochs, as summarised in Table 5. In the first stage (the pre-training stage), the network was a single-scale-channel network based on $\sigma_0 = 1$, while in the second stage (the post-training stage) the training process was then restarted, with the learned weights used to initialise the corresponding multi-scale-channel networks.

Crucially, the pre-trained networks in this section used the same total number of training epochs as the genuine multi-scale-channel trained networks in Section 6 in the main body of the paper, to show the relative efficiency of this approach.⁹ Furthermore, the first stage of training with a single-scale-channel network required far less GPU memory, thereby allowing for a larger batch size, which leads to faster training and improved generalisation.

The results of these experiments are shown in Figure 21, where the scale generalisation curves of the pre-trained networks are compared to the networks trained in the standard multi-scale-channel manner. During the

⁸ In this case the word "pre-training" refers to the fact that single-scale-channel training is performed before later fine-tuning with multi-scale-channel training, a process that does not involve the use of any additional dataset.

⁹ Probably, longer training could improve the results further.

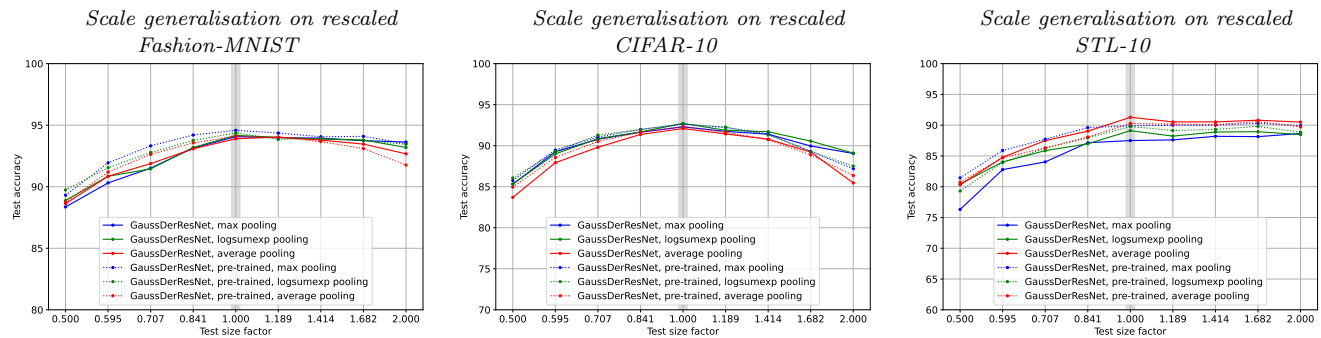


Fig. 21: Comparison between the scale generalisation curves for the multi-scale-channel GaussDerResNets trained using either pre-training or genuine multi-scale-channel training, with all the networks based on max pooling over scales, on the rescaled (a) Fashion-MNIST, (b) CIFAR-10 and (c) STL-10 datasets. The networks were trained on size factor 1 training data, and then evaluated on rescaled test datasets for each of the size factors between 1/2 and 2. As can be seen from the graphs, pre-training improves the performance for the smaller size factors for all the three rescaled datasets, while for the larger size factors the effect varies. The pre-training improves the performance in some cases or reducing it slightly in other. Note that the vertical axes for the test accuracy use different lower bounds for the different datasets.

Training Parameters	rescaled Fashion-MNIST	rescaled CIFAR-10	rescaled STL-10
Number of first stage epochs	16	40	50
Number of second stage epochs	16	50	70
Batch size during first stage	128	128	64
Batch size during second stage	64	45	17
Initial learning rate (first stage)	0.01	0.01	0.01
Initial learning rate (second stage)	0.005	0.005	0.005

Table 5: Training configurations for pre-training with single-scale-channel of GaussDerResNets employed in our experiments, for the three rescaled datasets.

evaluation of the network for the rescaled STL-10 dataset, the networks additionally used an extra boundary scale channel, based on $\sigma_0 = 2\sqrt[4]{2}$, because, as we will see in Appendix A.5, this was found to improve the scale generalisation at the larger size factors.

For the rescaled Fashion-MNIST dataset, we can see clear improvements in both the performance and the scale generalisation for the pre-trained GaussDerResNets, with the most notable improvement found for the size factors ≤ 1 , especially for max and logsumexp scale pooling. Similar results are seen for the rescaled CIFAR-10 dataset, with the pre-trained networks showing minor improvement in the test accuracy for the smaller size factors, and a slight drop in the performance for the larger size factors, here for the networks based on max pooling and logsumexp pooling.

For the rescaled STL-10 dataset, we again find that pre-training results in greatly improved performance for the smaller size factors. The improvement is most notable for the network based on max pooling, achieving very good performance and scale generalisation. The network based on logsumexp pooling also benefits somewhat from pre-training, while the average pooling net-

work works better when trained in a standard way, as it already has stable convergence.

These results show that this two-stage training approach not only requires much less computational resources during training, but that it can also improve the accuracy and the scale generalisation. It provides a balanced middle ground between the efficient single-scale-channel training, where features at a single scale can be learned effectively, and multi-scale-channel training, where optimisation is done over several scales at once, which is crucial for the network to learn how to automatically adapt to and handle interactions between the different scale channels.

Let us finally remark that multi-scale-channel optimisation is non-trivial. Here, we have shown that including a single-scale-channel pre-training stage provides valuable initial guidance during the training process, which is especially beneficial for the smaller size factors, since it avoids suboptimal convergence during training, which would negatively affect the performance.

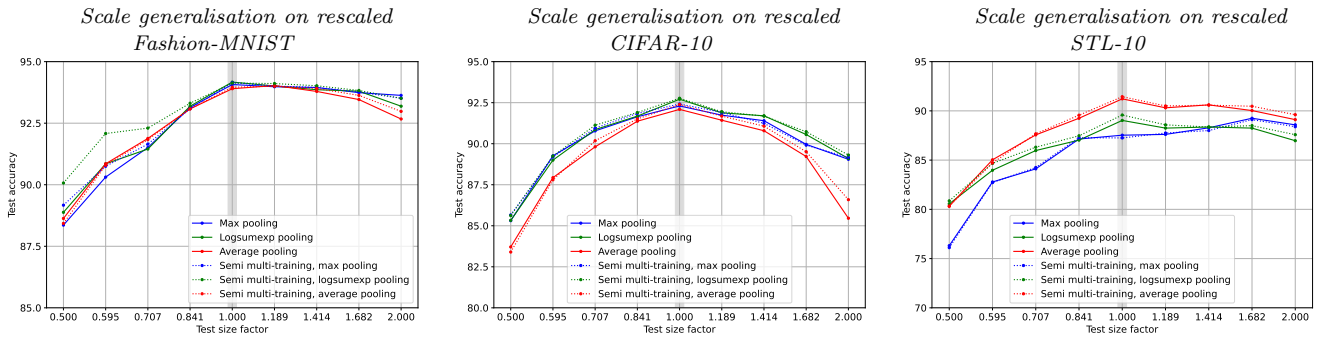


Fig. 22: Comparison between the zoomed in scale generalisation curves for the multi-scale-channel GaussDerResNets and for the GaussDerResNets extended after training using weight transfer to have additional scale channels that cover a denser scale sampling of the scale levels, with the networks based on max, logsumexp or average pooling over scales, on the rescaled (left) Fashion-MNIST, (middle) CIFAR-10 and (right) STL-10 datasets. The training was performed on training data at size factor 1, and inference was performed on test data for each of the size factors between 1/2 and 2. From the graphs, we can see that in general networks with more scale-channels tend to have marginally improved scale generalisation. Note that the vertical axes for the test accuracy use different lower bounds for the different datasets.

A.5 Impact of semi-multi-scale-channel training

Multi-scale-channel training has been demonstrated to achieve better scale generalisation compared to weight transfer from a single-scale-channel network trained on fixed object size, but it can be computationally costly. A middle ground between these two methods, which we refer to as semi-multi-scale-channel training, is when a multi-scale-channel network with a certain scale channel spacing is trained, and then during inference the weights are transferred to a multi-scale-channel network with a denser scale sampling of the scale levels. This approach retains the benefits of multi-scale-channel training, while reducing the required computational resources for optimising the GaussDerResNets with the denser distribution of scale channels. In this section, we compare the scale generalisation properties of GaussDerResNets with a denser scale sampling of the scale levels trained using semi-multi-scale-channel training, to GaussDerResNets trained using standard scale-channel spacing.

We use $\lambda = \sqrt{2}$ as the spacing factor between neighbouring scale channels during training, and during inference we transfer the weights to a network with scale level sampling ratio of $\sqrt[4]{2}$. Specifically, we take a trained network based on $\sigma_{i,0} \in \{1/(2\sqrt{2}), 1/2, 1/\sqrt{2}, 1, \sqrt{2}, 2\}$, and transfer its weights to a network based on $\sigma_{i,0} \in \{1/(2\sqrt{2}), 1/(2\sqrt[4]{2}), \dots, 2, 2\sqrt[4]{2}\}$, which matches the scale spacing of the test sets of the rescaled datasets we use.

The results are shown in Figure 22, for the rescaled Fashion-MNIST, CIFAR-10 and STL-10 datasets.

For all the three datasets, we can see that semi-multi-scale-channel training results in minor improvements to the scale generalisation performance. In sev-

eral cases, we can also see that the addition of the extra large boundary scale channel during the inference stage clearly does help improve generalisation for larger size factors. One clear case, where the use of a denser scale channel sampling is found to be helpful, is in the leftmost plot for the rescaled Fashion-MNIST experiment, where the scale generalisation of the logsumexp based network improved significantly, especially for the smaller size factors.

Additionally, we can see that even for a less dense scale-channel spacing, the scale channels cover the in-between range of scales quite well, and not only the exact scale they are defined for using the initial scale level. This means that the scale generalisation curve does not fluctuate (for the most part), despite the discrete sampled scale levels.

A.6 Visualisation of the learned receptive fields

To provide further insight into the learned representations GaussDerResNets, we visualise the effective filters across the network layers, for the GaussDerResNets with the computational primitives of the layers extended to also include zero-order terms and trained on the rescaled STL-10 dataset, illustrating the progression from low-level to intermediate and deep hierarchical features. These receptive fields are computed as linear combinations of a scale-normalised Gaussian derivative kernel basis, here including the zero-order term and using spatial max pooling in the training stage.

The discrete kernel basis for the filters in that model is computed using the discrete analogue of Gaussian kernel, with the Gaussian derivatives computed using

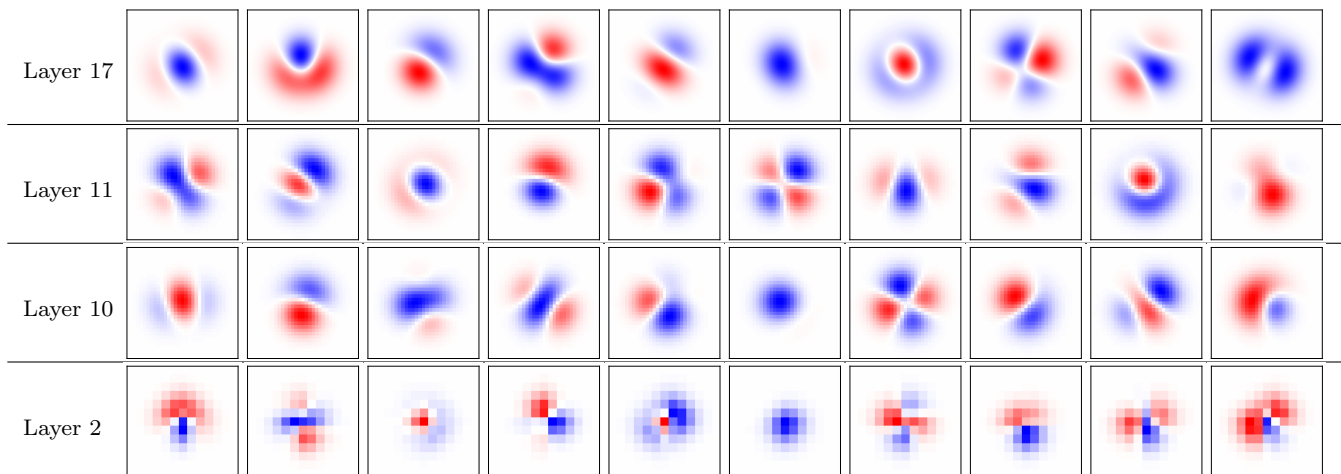


Fig. 23: A representative showcase of 10 learned effective filters from an early layer, two intermediate layers from a single residual block and the penultimate layer (specifically the 2nd, 10th, 11th and 17th layers) of a single-scale-channel GaussDerResNet with a zero-order term included in the filter basis, and trained on the rescaled STL-10 dataset. The colour mapping is configured such that zero values appear white, positive values are shown in red, and negative values are represented in blue. The size of these convolution kernels becomes larger in the higher layers, as the consequence of the scale parameter σ increasing with depth according to Equation (29). We can see that the learned filters are not always DC balanced, and that some of them are similar to different directional derivatives or the Laplacian-of-Gaussian.

central difference operators, as described in Section 3.9 in the main body of the paper. While all the scale channels share the same weights, we showcase the filters specifically for the scale channel based on the initial scale value $\sigma_0 = 1$.

The extracted receptive fields are shown in Figure 23. As can be seen, some of the filters are similar to directional derivatives of Gaussian kernels or Laplacians-of-Gaussians. The variability in the shapes of the filters is, however, substantially richer than plain Gaussian derivatives or Laplacians-of-Gaussians. Furthermore, due to the inclusion of the zero-order term in the layers of the network, the receptive fields are not always DC-balanced, meaning that the masses of the positive and the negative parts may not always be equal.

References

- Abramowitz, M. and Stegun, I. A. (eds.) (1964). *Handbook of Mathematical Functions*. Applied Mathematics Series (National Bureau of Standards), 55 edn.
- Alt, T., Schrader, K., Augustin, M., Peter, P., and Weickert, J. (2023). Connections between numerical algorithms for PDEs and neural networks. *Journal of Mathematical Imaging and Vision* 65, 185–208
- Babaiee, Z., Kiasari, P., Rus, D., and Grosu, R. (2024a). We need far fewer unique filters than we thought. In *NeurIPS 2024 Workshop on Scientific Methods for Understanding Deep Learning*. <https://openreview.net/pdf?id=RV8oJTkqkj>
- Babaiee, Z., Kiasari, P., Rus, D., and Grosu, R. (2025). The master key filters hypothesis: Deep filters are general. In *AAAI Conference on Artificial Intelligence*. arXiv preprint arXiv:2412.16751
- Babaiee, Z., Kiasari, P. M., Rus, D., and Grosu, R. (2024b). Unveiling the unseen: Identifiable clusters in trained depth-wise convolutional kernels. In *International Conference for Learning Representations (ICLR 2024)*. arXiv preprint arXiv:2401.14469
- Barisin, T., Angulo, J., Schladitz, K., and Redenbach, C. (2024a). Riesz feature representation: Scale equivariant scattering network for classification tasks. *SIAM Journal on Imaging Sciences* 17, 1284–1313
- Barisin, T., Schladitz, K., and Redenbach, C. (2024b). Riesz networks: Scale invariant neural networks in a single forward pass. *Journal of Mathematical Imaging and Vision* 66, 246–270
- Basting, M., Brintjes, R.-J., Wiedemer, T., Kümmerer, M., Bethge, M., and van Gemert, J. (2024). Scale learning in scale-equivariant convolutional networks. In *Proceedings of the 19th International Joint Conference on Computer Vision, Imaging and Computer Graphics Theory and Applications - Volume 2: VISAPP*. 567–574
- Bay, H., Ess, A., Tuytelaars, T., and van Gool, L. (2008). Speeded up robust features (SURF). *Computer Vision and Image Understanding* 110, 346–359
- Bekkers, E. J. (2020). B-spline CNNs on Lie groups. *International Conference on Learning Representations (ICLR 2020)*
- Bellaard, G., Sakata, S., Smets, B. M., and Duits, R. (2025). PDE-CNNs: Axiomatic derivations and applications. *Journal of Mathematical Imaging and Vision* 67, 13:1–25
- Bretzner, L. and Lindeberg, T. (1998). Feature tracking with automatic selection of spatial scales. *Computer Vision and Image Understanding* 71, 385–392
- Bronstein, M. M., Bruna, J., Cohen, T., and Velicković, P. (2021). Geometric deep learning: Grids, groups, graphs, geodesics, and gauges. *arXiv preprint arXiv:2104.13478*
- Brintjes, R.-J., Motyka, T., and van Gemert, J. (2023). What affects learned equivariance in deep image recognition models? In *Proceedings Computer Vision and Pattern Recognition (CVPR 2023)*. 4839–4847
- Bruna, J. and Mallat, S. (2013). Invariant scattering convolution networks. *IEEE Trans. Pattern Analysis and Machine*

- Intell.* 35, 1872–1886
- Chen, Y., Fang, H., Xu, B., Yan, Z., Kalantidis, Y., Rohrbach, M., et al. (2019). Drop an octave: Reducing spatial redundancy in convolutional neural networks with octave convolution. In *Proc. International Conference on Computer Vision (ICCV 2019)*
- Cho, T., Nam, H., and Choi, J. (2025). Scale-equivariant object perception for autonomous driving. *IEEE Transactions on Intelligent Vehicles* 10, 4361–4370
- Chollet, F. (2017). Xception: Deep learning with depthwise separable convolutions. In *Proc. Computer Vision and Pattern Recognition (CVPR 2017)*. 1800–1807
- Coates, A., Ng, A., and Lee, H. (2011). An analysis of single-layer networks in unsupervised feature learning. In *Proc. 14:th International Conference on Artificial Intelligence and Statistics*. 215–223
- Courtois, A., Morel, J.-M., and Arias, P. (2023). Can neural networks extrapolate? Discussion of a theorem by Pedro Domingos. *Revista de la Real Academia de Ciencias Exactas, Físicas y Naturales. Serie A. Matemáticas* 117, 79
- Dai, Z., Liu, H., Le, Q. V., and Tan, M. (2021). CoAtNet: Marrying convolution and attention for all data sizes. *Advances in Neural Information Processing Systems* 34, 3965–3977
- Domingos, P. (2020). Every model learned by gradient descent is approximately a kernel machine. *arXiv preprint arXiv:2012.00152*
- Fu, Y., Zhang, P., Liu, B., Rong, Z., and Wu, Y. (2022). Learning to reduce scale differences for large-scale invariant image matching. *IEEE Transactions on Circuits and Systems for Video Technology* 33, 1335–1348
- Gavilima-Pilatáxi, H. and Ibarra-Fiallo, J. (2023). Multi-channel Gaussian derivative neural networks for crowd analysis. In *Proc. International Conference on Pattern Recognition Systems (ICPRS 2023)*. 1–7
- Gerken, J. E., Aronsson, J., Carlsson, O., Linander, H., Ohlsson, F., Petersson, C., et al. (2023). Geometric deep learning and equivariant neural networks. *Artificial Intelligence Review* 56, 14605–14662
- Ghosh, R. and Gupta, A. K. (2019). Scale steerable filters for locally scale-invariant convolutional neural networks. *ICML Workshop on Theoretical Physics for Deep Learning arXiv preprint arXiv:1906.03861*
- He, K., Zhang, X., Ren, S., and Sun, J. (2016). Deep residual learning for image recognition. In *Proc. Computer Vision and Pattern Recognition (CVPR 2016)*. 770–778
- Howard, A. G., Zhu, M., Chen, B., Kalenichenko, D., Wang, W., Weyand, T., et al. (2017). MobileNets: Efficient convolutional neural networks for mobile vision applications. *arXiv preprint arXiv:1704.04861*
- Iijima, T. (1962). Basic theory on normalization of pattern (in case of typical one-dimensional pattern). *Bulletin of the Electrotechnical Laboratory* 26, 368–388. (in Japanese)
- Jacobsen, J.-J., van Gemert, J., Lou, Z., and Smeulders, A. W. M. (2016). Structured receptive fields in CNNs. In *Proc. Computer Vision and Pattern Recognition (CVPR 2016)*. 2610–2619
- Jansson, Y. and Lindeberg, T. (2022). Scale-invariant scale-channel networks: Deep networks that generalise to previously unseen scales. *Journal of Mathematical Imaging and Vision* 64, 506–536
- Kanazawa, A., Sharma, A., and Jacobs, D. W. (2014). Locally scale-invariant convolutional neural networks. *NIPS 2014 Deep Learning and Representation Learning Workshop arXiv preprint arXiv:1412.5104*
- Koenderink, J. J. (1984). The structure of images. *Biological Cybernetics* 50, 363–370
- Koenderink, J. J. and van Doorn, A. J. (1992). Generic neighborhood operators. *IEEE Trans. Pattern Analysis and Machine Intell.* 14, 597–605
- Krizhevsky, A. and Hinton, G. (2009). *Learning multiple layers of features from tiny images*. Tech. rep., University of Toronto
- Lindeberg, T. (1990). Scale-space for discrete signals. *IEEE Trans. Pattern Analysis and Machine Intell.* 12, 234–254
- Lindeberg, T. (1993). *Scale-Space Theory in Computer Vision* (Springer)
- Lindeberg, T. (1998a). Edge detection and ridge detection with automatic scale selection. *International Journal of Computer Vision* 30, 117–154
- Lindeberg, T. (1998b). Feature detection with automatic scale selection. *International Journal of Computer Vision* 30, 77–116
- Lindeberg, T. (2011). Generalized Gaussian scale-space axiomatics comprising linear scale-space, affine scale-space and spatio-temporal scale-space. *Journal of Mathematical Imaging and Vision* 40, 36–81
- Lindeberg, T. (2013a). A computational theory of visual receptive fields. *Biological Cybernetics* 107, 589–635
- Lindeberg, T. (2013b). Generalized axiomatic scale-space theory. In *Advances in Imaging and Electron Physics*, ed. P. Hawkes (Elsevier), vol. 178. 1–96
- Lindeberg, T. (2013c). Scale selection properties of generalized scale-space interest point detectors. *Journal of Mathematical Imaging and Vision* 46, 177–210
- Lindeberg, T. (2015). Image matching using generalized scale-space interest points. *Journal of Mathematical Imaging and Vision* 52, 3–36
- Lindeberg, T. (2020). Provably scale-covariant continuous hierarchical networks based on scale-normalized differential expressions coupled in cascade. *Journal of Mathematical Imaging and Vision* 62, 120–148
- Lindeberg, T. (2021a). Normative theory of visual receptive fields. *Heliyon* 7, e05897:1–20. doi:10.1016/j.heliyon.2021.e05897
- Lindeberg, T. (2021b). Scale selection. In *Computer Vision*, ed. K. Ikeuchi (Springer). 1110–1123. https://doi.org/10.1007/978-3-030-03243-2_242-1
- Lindeberg, T. (2022). Scale-covariant and scale-invariant Gaussian derivative networks. *Journal of Mathematical Imaging and Vision* 64, 223–242
- Lindeberg, T. (2023). Covariance properties under natural image transformations for the generalized Gaussian derivative model for visual receptive fields. *Frontiers in Computational Neuroscience* 17, 1189949:1–23
- Lindeberg, T. (2024). Discrete approximations of Gaussian smoothing and Gaussian derivatives. *Journal of Mathematical Imaging and Vision* 66, 759–800
- Lindeberg, T. (2025a). Approximation properties relative to continuous scale space for hybrid discretizations of Gaussian derivative operators. *Frontiers in Signal Processing* 4, 1447841:1–12. doi:10.3389/frsip.2024.1447841
- Lindeberg, T. (2025b). Unified theory for joint covariance properties under geometric image transformations for spatio-temporal receptive fields according to the generalized Gaussian derivative model for visual receptive fields. *Journal of Mathematical Imaging and Vision* 67, 44:1–49
- Lindeberg, T., Babaiee, Z., and Kiasari, P. M. (2025). Modelling and analysis of the 8 filters from the “master key filters hypothesis” for depthwise-separable deep networks in relation to idealized receptive fields based on scale-space

- theory. *arXiv preprint arXiv:2509.12746*
- Liu, Z., Mao, H., Wu, C.-Y., Feichtenhofer, C., Darrell, T., and Xie, S. (2022). A ConvNet for the 2020s. In *Proc. Computer Vision and Pattern Recognition (CVPR 2022)*. 11976–11986
- Lowe, D. G. (2004). Distinctive image features from scale-invariant keypoints. *International Journal of Computer Vision* 60, 91–110
- Lu, Y., Zhong, A., Li, Q., and Dong, B. (2018). Beyond finite layer neural networks: Bridging deep architectures and numerical differential equations. In *International Conference on Machine Learning (ICML 2018)* (PMLR), 3276–3285
- Mallat, S. (2016). Understanding deep convolutional networks. *Phil. Trans. Royal Society A* 374, 20150203
- Manolache, A., Chamon, L. F. O., and Niepert, M. (2025). Learning (approximately) equivariant networks via constrained optimization. In *Proc. Neural Information Processing Systems (NeurIPS 2025)*. Preprint at arXiv:2505.13631
- Marcos, D., Kellenberger, B., Lobry, S., and Tuia, D. (2018). Scale equivariance in CNNs with vector fields. *ICML/FAIM 2018 Workshop on Towards Learning with Limited Labels: Equivariance, Invariance, and Beyond* arXiv preprint arXiv:1807.11783
- Mondal, A. K., Panigrahi, S. S., Kaba, O., Mudumba, S. R., and Ravanbakhsh, S. (2023). Equivariant adaptation of large pretrained models. *Advances in Neural Information Processing Systems (NeurIPS 2023)* 36, 50293–50309
- Moskalev, A., Sepiarskaia, A., Bekkers, E. J., and Smeulders, A. W. M. (2023). On genuine invariance learning without weight-tying. In *Topological, Algebraic and Geometric Learning Workshops*. 218–227
- Müller, R., Kornblith, S., and Hinton, G. E. (2019). When does label smoothing help? *Advances in Neural Information Processing Systems (NeurIPS 2019)* 32
- Nordenfors, O. and Flinth, A. (2024). Ensembles provably learn equivariance through data augmentation. *arXiv preprint arXiv:2410.01452*
- Pant, N., Rodriguez, I. F., Beniwal, A., Warren, S., and Serre, T. (2024). HMAX strikes back: Self-supervised learning of human-like scale invariant representations. In *7th Annual Conference on Cognitive Computational Neuroscience*
- Penaud-Polge, V., Velasco-Forero, S., and Angulo, J. (2022). Fully trainable Gaussian derivative convolutional layer. In *International Conference on Image Processing (ICIP 2022)*. 2421–2425
- Perin, A. and Deny, S. (2025). On the ability of deep networks to learn symmetries from data: A neural kernel theory. *Journal of Machine Learning Research* 26, 1–70
- Pertigkiozoglou, S., Chatzipantazis, E., Trivedi, S., and Dailidis, K. (2024). Improving equivariant model training via constraint relaxation. *Advances in Neural Information Processing Systems (NeurIPS 2024)* 37, 83497–83520
- Perzanowski, A. and Lindeberg, T. (2025a). Rescaled CIFAR-10 dataset. *Zenodo* doi:10.5281/zenodo.15188748
- Perzanowski, A. and Lindeberg, T. (2025b). Rescaled Fashion-MNIST dataset. *Zenodo* doi:10.5281/zenodo.15187793
- Perzanowski, A. and Lindeberg, T. (2025c). Scale generalisation properties of extended scale-covariant and scale-invariant Gaussian derivative networks on image datasets with spatial scaling variations. *Journal of Mathematical Imaging and Vision* 67, 1–39
- Pintea, S. L., Tömen, N., Goes, S. F., Loog, M., and van Gemert, J. C. (2021). Resolution learning in deep convolutional networks using scale-space theory. *IEEE Trans. Image Processing* 30, 8342–8353
- Rahman, M. A., Yang, C.-A., Cheng, M., Hao, L. J., Jiang, J., Lim, T.-Y., et al. (2025). Local scale equivariance with latent deep equilibrium canonicalizer. In *Proc. International Conference on Computer Vision (ICCV 2025)*
- Ruthotto, L. and Haber, E. (2020). Deep neural networks motivated by partial differential equations. *Journal of Mathematical Imaging and Vision* 62, 352–364
- Sangalli, M., Blusseau, S., Velasco-Forero, S., and Angulo, J. (2022a). Differential invariants for SE(2)-equivariant networks. In *International Conference on Image Processing (ICIP 2022)*. 2216–2220
- Sangalli, M., Blusseau, S., Velasco-Forero, S., and Angulo, J. (2022b). Scale equivariant U-net. In *Proc. British Machine Vision Conference (BMVC 2022)*
- Shewmake, C., Buracas, D., Lillemark, H., Shin, J., Bekkers, E., Miolane, N., et al. (2023). Visual scene representation with hierarchical equivariant sparse coding. In *Proceedings of Machine Learning Research—NeurIPS workshops*
- Singh, B., Najibi, M., Sharma, A., and Davis, L. S. (2022). Scale normalized image pyramids with AutoFocus for object detection. *IEEE Trans. Pattern Analysis and Machine Intell.* 44, 3749–3766
- Smets, B. M. N., Portegies, J., Bekkers, E. J., and Duits, R. (2023). PDE-based group equivariant convolutional neural networks. *Journal of Mathematical Imaging and Vision* 65, 209–239
- Sosnovik, I., Moskalev, A., and Smeulders, A. (2021). DISCO: Accurate discrete scale convolutions. *British Machine Vision Conference (BMVC 2021)* arXiv preprint arXiv:2106.02733
- Sosnovik, I., Szmaja, M., and Smeulders, A. (2020). Scale-equivariant steerable networks. *International Conference on Learning Representations (ICLR 2020)*
- Tan, M. and Le, Q. V. (2021). EfficientNetV2: Smaller models and faster training. *International Conference on Machine Learning (ICML 2021)* arXiv preprint arXiv:2104.00298
- Ulicny, M., Krylov, V. A., and Dahyot, R. (2019). Harmonic networks with limited training samples. In *2019 27th European Signal Processing Conference (EUSIPCO)*. 1–5
- van der Ouderaa, T., Immer, A., and van der Wilk, M. (2023). Learning layer-wise equivariances automatically using gradients. *Advances in Neural Information Processing Systems (NeurIPS 2023)* 36, 28365–28377
- Wang, X., Zhang, S., Yu, Z., Feng, L., and Zhang, W. (2020). Scale-equalizing pyramid convolution for object detection. In *Proc. Computer Vision and Pattern Recognition (CVPR 2020)*. 13359–13368
- Weickert, J., Ishikawa, S., and Imiya, A. (1999). Linear scale-space has first been proposed in Japan. *Journal of Mathematical Imaging and Vision* 10, 237–252
- Wimmer, T., Golkov, V., Dang, H. N., Zaiss, M., Maier, A., and Cremers, D. (2023). Scale-equivariant deep learning for 3D data. *arXiv preprint arXiv:2304.05864*
- Wolski, K., Djeacoumar, A., Javanmardi, A., Seidel, H.-P., Theobalt, C., Cordonnier, G., et al. (2024). Learning images across scales using adversarial training. *ACM Transactions on Graphics (SIGGRAPH)* 43, 131
- Woo, S., Debnath, S., Hu, R., Chen, X., Liu, Z., Kweon, I. S., et al. (2023). ConvNeXt V2: Co-designing and scaling ConvNets with masked autoencoders. In *Computer Vision and Pattern Recognition (CVPR 2023)*
- Worrall, D. and Welling, M. (2019). Deep scale-spaces: Equivariance over scale. In *Advances in Neural Information Processing Systems (NeurIPS 2019)*. 7366–7378
- Xiao, H., Rasul, K., and Vollgraf, R. (2017). Fashion-MNIST: A novel image dataset for benchmarking machine learning

-
- algorithms. *arXiv preprint arXiv:1708.07747*
- Xu, S., Venugopalan, S., and Sundararajan, M. (2020). Attribution in scale and space. In *Proc. Computer Vision and Pattern Recognition (CVPR 2020)*. 9680–9689
- Xu, S., Wang, Y., Luo, X., Yoon, B.-J., and Qian, X. (2025). Scale-invariant implicit neural representations for object counting. In *Proc. Computer Vision and Pattern Recognition Conference (CVPR 2025)*. 2308–2318
- Xu, Y., Xiao, T., Zhang, J., Yang, K., and Zhang, Z. (2014). Scale-invariant convolutional neural networks. *arXiv preprint arXiv:1411.6369*
- Yang, Y., Dasmahapatra, S., and Mahmoodi, S. (2022). Scale-equivariant UNet for histopathology image segmentation. *Proceedings of Machine Learning Research* 194, 130–148
- Zagoruyko, S. and Komodakis, N. (2016). Wide residual networks. In *Proceedings of the British Machine Vision Conference (BMVC 2016)*. 87.1–87.12. doi:10.5244/C.30.87
- Zhan, W., Sun, G., and Li, Y. (2022). Scale-equivariant steerable networks for crowd counting. In *Proc. International Conference on Control and Robotics Engineering (IC-CRE 2022)*. 174–179
- Zhang, J., Li, G., Su, Q., Cao, L., Tian, Y., and Xu, B. (2025). Enabling scale and rotation invariance in convolutional neural networks with retina like transformation. *Neural Networks* , 107395
- Zhong, Y., Zhou, W., and Wang, Z. (2025). A survey of data augmentation in domain generalization. *Neural Processing Letters* 57, 34
- Zhu, W., Qiu, Q., Calderbank, R., Sapiro, G., and Cheng, X. (2022). Scale-translation-equivariant neural networks with decomposed convolutional filters. *Journal of Machine Learning Research* 23, 1–45